

SPHY v2.0: Spatial Processes in Hydrology

Model theory, installation, and data
preparation

October 2015



Author

W. Terink
A.F. Lutz
W.W. Immerzeel

Report FutureWater: 142



FutureWater

Costerweg 1V
6702 AA Wageningen
The Netherlands

+31 (0)317 460050

info@futurewater.nl

www.futurewater.nl

Acknowledgements

The development and publication of the SPHY model source code, its binaries, GUIs, and case-studies has been supported through various (research) projects that were partly or completely funded by the following organizations:

- International Centre for Integrated Mountain Development (ICIMOD¹);
- European Space Agency (ESA²);
- Asian Development Bank (ADB³);
- World Bank⁴;
- Rijksdienst voor Ondernemend Nederland (RVO⁵)
- NUFFIC⁶

We are very grateful to these organizations that made the development of the SPHY model possible. We hope to continue to collaborate with these organizations in the future in order to further develop and improve the SPHY model and its interfaces.

¹ <http://www.icimod.org/>

² <http://www.esa.int/ESA>

³ <http://www.adb.org/>

⁴ <http://www.worldbank.org/>

⁵ <http://www.rvo.nl/>

⁶ <https://www.nuffic.nl/en>



Table of contents

Acknowledgements	2
1 Introduction	7
2 Theory	10
2.1 Background	10
2.2 Modules	12
2.3 Reference and potential evapotranspiration	13
2.4 Dynamic vegetation processes	14
2.4.1 Maximum canopy storage	14
2.4.2 Interception	15
2.5 Snow processes	16
2.5.1 Snow and rainfall	16
2.5.2 Snowmelt, refreezing, and storage	17
2.5.3 Snow runoff	18
2.6 Glacier processes	18
2.6.1 Glacier melt	18
2.6.2 Glacier runoff	19
2.6.3 Glacier percolation	19
2.7 Soil water processes	19
2.7.1 Soil water balances	19
2.7.2 Actual evapotranspiration	20
2.7.3 Surface runoff	21
2.7.4 Lateral flow	22
2.7.5 Percolation	23
2.7.6 Groundwater recharge	23
2.7.7 Baseflow	24
2.8 Routing	25
2.8.1 Runoff routing	25
2.8.2 Lake/reservoir routing	26
3 Applications	28
3.1 Irrigation management in lowland areas	28
3.2 Snow- and glacier-fed river basins	30
3.3 Flow forecasting	34
4 Installation of SPHY	38
4.1 General	38
4.2 Installing SPHY as a stand-alone application	38
4.2.1 Python 2.7.6 32-bit	38
4.2.2 Numpy 1.8.0 32-bit	40
4.2.3 PCRaster 4.0 32-bit	41
4.2.4 SPHY v2.0 source code	43
5 Build your own SPHY-model	44
5.1 Select projection extent and resolution	44
5.2 Clone map	44
5.3 DEM and Slope	45
5.4 Delineate catchment and create local drain direction map	50
5.5 Preparing stations map and sub-basins.map	51
5.6 Glacier fraction map	56



5.7	Other static input maps	58
5.8	Meteorological forcing map series	59
6	References	60
	Copyright	70



Tables

Table 1: Pros (+) and cons (-) of some well-known hydrological models, including the SPHY model. A categorization is made between (i) processes that are integrated, (ii) field of application, (iii) scale of application, and (iv) implementation.	9
Table 2: LAI _{max} values for different vegetation types (Sellers et al., 1996).	15
Table 3: Station locations used for calibration and validation of the SPHY model in HICAP (Lutz et al., 2014a). Three stations were used for calibration for 1998–2007. Five stations were used for an independent validation for the same period. The Nash–Sutcliffe efficiency (NS) and bias metrics were calculated at a monthly time step.	32
Table 4: Resampling settings based on the layer data type.	49
Table 5: Data types used in SPHY.	59
Table 6: Overview of SPHY model parameters. The last column indicates whether the parameter is observable, or can be determined by calibration (free).....	71

Figures

Figure 1: Illustration of SPHY sub-grid variability. A grid cell in SPHY can be (a) partially covered with glaciers, or (b) completely covered with glaciers, or (c1) free of snow, or (c2) completely covered with snow. In the case of (c1), the free land surface can consist of bare soil, vegetation, or open water.	10
Figure 2: SPHY modeling concepts. The fluxes in grey are only incorporated when the groundwater module is not used. Abbreviations are explained in the text.....	11
Figure 3: Modules of the SPHY model that can be switched on/off.....	13
Figure 4: Spatial distribution of evapotranspiration (ET) deficit, as simulated by the SPHY model for a Romanian farm on 03 April 2014. Transparency means no ET deficit.	29
Figure 5: Measured and simulated daily root-zone soil moisture content during the 2014 growing season. Rainfall+irrigation has been measured by the rain gauge that was attached to the moisture sensor.	30
Figure 6: Average monthly observed and SPHY-simulated flow (1998–2007) for the Chatara major discharge measurement location in the Ganges basin (Lutz et al. 2014a). Metrics are calculated based on monthly time steps.	31
Figure 7: The contribution of glacier melt (a), snowmelt (b), and rainfall (c) to the total flow for major streams in the upstream basins of the Indus, Ganges, Brahmaputra, Salween and Mekong during 1998–2007 (Lutz et al. 2014a).	32
Figure 8: Observed and simulated average fractional snow cover in the upper Indus basin. The values represent the 9-year average for 46 (8-day) periods during 2000–2007.....	33
Figure 9: (a) SPHY simulated snow cover 2000–2007 and (b) MODIS observed snow cover 2000–2007.....	33
Figure 10: Snow storage (mm) as simulated by the SPHY model on 12 August (left) and 01 October (right) during the snow melting season of 2013 in the Laja River basin.	35
Figure 11: Daily observed vs. SPHY simulated streamflow (period 2007–2008) for the streamflow stations Canal Abanico (ID 19) and Rio Laja en Tucapel (ID 23). The Nash–Sutcliffe (NS) and bias model performance indicators are shown as well.	36
Figure 12: Bias between total cumulative forecasted flow and observed flow for the 23 model runs that were executed between the end of September 2013 and March 2014. Results are shown for the locations Canal Abanico (ID 19) and Rio Laja en Tucapel (ID 23).....	36



Figure 13: System properties to set Environmental Variables.	39
Figure 14: Setting the Path variable.	40
Figure 15: Adding the Python27 installation folder to the Path system variables.	40
Figure 16: Illustration of selecting the Python installation folder during installation of the Numpy package.	41
Figure 17: Adding the PCRaster bin folder to the Path system variables.	42
Figure 18: Editing or creating the PYTHONPATH variable for the PCRaster package.	42
Figure 19: Command prompt view of testing a successful installation of PCRaster after entering the <i>pcrcalc</i> command.	43
Figure 20: Command line menu for clone creation	45
Figure 21: Opening the “Processing Toolbox”.	45
Figure 22: Selecting the “Advanced interface” in the “Processing Toolbox”.	46
Figure 23: Warp tool.....	47
Figure 24: Setting the files and Source and Target SRS in the Warp Tool.....	47
Figure 25: Selecting the Resampling tool in the Processing Toolbox.....	48
Figure 26: Setting the Resampling tool options.	48
Figure 27: Translate tool (convert raster format).....	49
Figure 28: Setting the Translate options.	50
Figure 29: Saving the translated raster as a PCRaster Raster File (*.map).	50
Figure 30: Create new shapefile layer	51
Figure 31: Setting the properties of the New Shapefile Layer.	52
Figure 32: Toggle Editing for Shapefiles.	52
Figure 33: Add Feature for Shapefiles.	53
Figure 34: Adding points to the locations Shapefile layer using the <i>accuflux.map</i>	53
Figure 35: Selecting the <i>v.to.rast.attribute</i> tool from the Processing Toolbox.	54
Figure 36: Setting the options in the <i>v.to.rast.attribute</i> tool.....	54
Figure 37: Editing the command for Translation.	55
Figure 38: Adding the “-ot Float32” syntax to the command for Translation.....	55
Figure 39: Reclassify tool.....	56
Figure 40: Reclassify tool dialog box	57
Figure 41: GRASS aggregation tool.....	58
Figure 42: GRASS aggregation tool dialog box	58



1 Introduction

The number and diversity of water-related challenges are large and are expected to increase in the future (Wagener et al. 2010; Lall 2014). Even today, the ideal condition of having the appropriate amount of good-quality water at the desired place and time is most often not satisfied (Biswas and Tortajada 2010; Droogers and Bouma 2014). It is likely that climate variability and change will intensify food insecurity by water shortages (Wheeler and Braun 2013), and loss of access to drinking water (Rockström et al. 2012). Current and future water-related challenges are location and time specific and can vary from impact of glacier dynamics (Immerzeel et al. 2011), economic and population growth (Droogers et al. 2012), floods or extended and more prolonged droughts (Dai 2011), amongst others.

In response to these challenges, hydrologists and water resource specialists are developing modeling tools to analyze, understand and explore solutions to support decision makers and operational water managers (Pechlivanidis et al. 2011). Despite difficulties in connecting the scientific advances in hydrological modeling with the needs of decision makers and water managers, progress has been made and there is no doubt that modeling tools are indispensable in what is called good “water governance” (Droogers and Bouma 2014; Liu et al. 2008).

The strength of hydrological models is that they can provide output at high temporal and spatial resolutions, and for hydrological processes that are difficult to observe on the large scale that they are generally applied on (Bastiaanssen et al. 2007). The most important aspect of applying models is in their use in exploring different scenarios, expressing for example, possible effects of changes in population and climate on the water cycle (Droogers and Aerts 2005). Models are also applied at the operational level to explore interventions (management scenarios) to be used by water managers and policy makers. Examples of this are changes in reservoir operation rules, water allocation between sectors, investment in infrastructure such as water treatment or desalination plants, and agricultural and irrigation practices. In other words: models enable hydrologists and water managers to change focus from a re-active towards a pro-active approach.

Over the past decades, the land surface and hydrologic communities have made substantial progress in understanding the spatial presentation of fluxes of water and energy (Abbott et al. 1986; Wigmosta et al., 1994; Van der Kwaak and Loague 2001; Rigon et al., 2006). Their efforts have led to the development of well-known hydrological models, such as, e.g., VIC (Liang et al. 1994, 1996), SWAT (Neitsch et al. 2009), TOPKAPI-ETH (Finger et al. 2011; Ragetti and Pellicciotti 2012; Ragetti et al. 2013; Ragetti et al. 2014), LISFLOOD (Van Der Knijff et al, 2010), SWIM (Krysanova et al. 2015; Krysanova et al. 2000; Krysanova et al., 1998), HYPE (Lindström et al. 2010), mHM (Samaniego et al., 2010), PCR-GLOBWB (Beek and Bierkens 2008; Bierkens and Beek 2009; Wada et al. 2010; Sperna Weiland et al. 2010), MIKE-SHE (Refshaard and Storm 1995; Oogathoo et al. 2008; Deb and Shukla 2011) and GEOTop (Rigon et al., 2006; Endrizzi et al. 2013; Endrizzi et al. 2011), amongst others. The number of existing hydrological models is probably in the tens of thousands (Droogers and Bouma 2014). Some existing model reviews cover a substantial number of models: IRRISOFT (Irrisoft 2014): 114; USGS (2014): 110; EPA (2014): 211; USACE (HEC 2014): 18.

All these hydrological models are different with respect to (i) the number and detail of hydrological processes that are integrated, (ii) their field and (iii) scale of application, and (iv) the way they are implemented. Whereas, for example, the SWIM (Krysanova et al. 2015;



Krysanova et al. 2000; Krysanova, Müller-Wohlfeil, and Becker 1998) and HYPE (Lindström et al. 2010) models both include all major hydrological processes, the SWIM model is typically developed for large-scale (large river basins to continental) applications, and the HYPE model operates on the sub-basin scale. Therefore, these models contain less detail, in contrast to fully distributed models operating at grid level, such as, e.g., GEOtop (Rigon et al., 2006; Endrizzi et al. 2013; Endrizzi et al. 2011) and TOPKAPI-ETH (Finger et al. 2011; Ragettli and Pellicciotti 2012; Ragettli et al. 2013; Ragettli et al. 2014). Models like, e.g., MIKE-SHE (Refshaard and Storm 1995; Oogathoo et al. 2008; Deb and Shukla 2011) and LISFLOOD (Van Der Knijff, Younis, and De Roo 2010) have the advantage of being flexible in terms of the spatial and temporal resolutions, but their disadvantages are that they do not include glacier processes and that they are not open source and therefore not available to the larger community.

It is clear that all these models have their pros and cons in terms of (i) processes integrated, (ii) field of application, (iii) scale of application, and (iv) implementation. Table 1 shows the pros and cons of some well-known hydrological models, including the Spatial Processes in Hydrology (SPHY) model. Over the last couple of years we have developed the SPHY model, and improved its usefulness by applying the model in various research projects. SPHY has been developed with the explicit aim of simulating terrestrial hydrology under various physiographical and hydroclimatic conditions by integrating key components from existing and well-tested models: HydroS (Droogers and Immerzeel 2010), SWAT (Neitsch et al. 2009), PCR-GLOBWB (Beek and Bierkens 2008; Bierkens and Beek 2009; Wada et al. 2010; Sperna Weiland et al. 2010), SWAP (Dam et al. 1997) and HimSim (Immerzeel et al. 2011). Based on Table 1 it is clear that SPHY (i) integrates most hydrologic processes, including glacier processes, (ii) has the flexibility to study a wide range of applications, including climate and land use change impacts, irrigation planning, and droughts, (iii) can be used for catchment- and river-basin-scale applications as well as farm- and country-level applications, and has a flexible spatial resolution, and (iv) can easily be implemented. Implementation of SPHY is relatively easy because (i) it is open source, (ii) input and output maps can directly be used in GIS, (iii) it is set up modular in order to switch on/off relevant/irrelevant processes and thus decreases model run time and data requirements, (iv) it needs only daily precipitation and temperature data as climate forcing, (v) it can be forced with remote sensing data, and (vi) it uses a configuration file that allows the user to change model parameters and choose the model output that needs to be reported.

The objectives of this manual are:

- Introduce and present the SPHY model (v2.0)
- Present the SPHY model (v2.0) theory and demonstrate some typical applications
- Provide the steps that are required to install the SPHY model as a standalone application
- Learn how-to prepare model data for a SPHY model for your own area of interest

The model source code is in the public domain (open access) and can be obtained from the SPHY model website free of charge (www.sphy-model.org). The peer-reviewed open-access publication of the SPHY model can be found at <http://www.geosci-model-dev.net/8/2009/2015/gmd-8-2009-2015.pdf> (Terink et al., 2015).



Table 1: Pros (+) and cons (-) of some well-known hydrological models, including the SPHY model. A categorization is made between (i) processes that are integrated, (ii) field of application, (iii) scale of application, and (iv) implementation.

	SPHY	TOPKAPI-ETH	SWAT	VIC	LIS-FLOOD	SWIM	HYPE	mHM	MIKE-SHE	PCRGLOB-WB	GEO-top
Processes integrated											
Rainfall-runoff	+	+	+	+	+	+	+	+	+	+	+
Evapotranspiration	+	+	+	+	+	+	+	+	+	+	+
Dynamic vegetation growth	+	-	+	+	+	+	a	NA	+	+	-
Unsaturated zone	+	+	+	+	+	+	+	+	+	+	+
Groundwater	+	-	+	+	+	+	+	+	+	+	+
Glaciers	+	+	-	-	-	+	+	-	-	-	+
Snow	+	+	+	+	+	+	+	+	+	+	+
Routing	+	+	+	+	+	+	+	+	+	+	+
Lakes incorporated into routing scheme	+	-	+	+	+	+	+	NA	+	+	-
Reservoir management	-	-	+	-	-	+	+	NA	-	+	-
Field of application											
Climate change impacts	+	+	+	+	+	+	+	+	+	+	+
Land use change impacts	+	+	+	+	+	+	+	+	+	+	+
Irrigation planning	+	-	+	+	-	+	+	-	+	-	+
Floods	-	-	-	-	c	-	+	-	+	+	+
Droughts	+	+	+	+	+	+	+	+	+	+	+
Water supply and demand	-	-	+	-	-	-	+	NA	-	-	-
Scale of application											
Catchment scale	+	+	+	+	-	-	+	-	+	-	+
River basin scale	+	+	+	+	+	+	+	+	+	-	-
Mesoscale river basins	+	-	+	+	+	+	+	+	+	+	-
Global scale	-	-	-	+	+	-	-	-	-	+	-
Farm level	+	-	-	-	-	-	+	-	-	-	-
Country level	+	-	-	-	-	-	+	-	-	-	-
Fully distributed	+	+	-	+	+	-	-	+	+	+	+
Sub-grid variability	+	-	-	+	-	-	-	+	-	+	+
Flexible spatial resolution	+	+	-	+	+	-	-	+	+	+	+
Hourly resolution	-	+	+	-	+	-	+	+	+	-	+
Sub-daily resolution	-	-	-	+	+	-	+	NA	+	-	-
Daily resolution	+	+	+	+	+	+	+	NA	+	+	-
Implementation											
Open source	+	-	+	+	-	-	+	-	-	-	+
Forcing with remote sensing	+	+	-	+	+	-	+	NA	-	-	+
GIS compatibility	+	+	+	-	+	+	+	+	+	+	+
Modular set up	+	-	-	+	+	+	+	+	+	-	-
Computational efficient	+	+	+	-	+	+	+	+	-	+	+
Climate forcing requirements	+	+	-	b	-	-	+	+	-	-	-
Flexible output reporting options	+	+	-	+	+	+	+	NA	+	-	+
Graphical user-interface in GIS	a	-	+	-	-	+	-	-	+	-	-

^a Currently in development. ^b More climate variables are required if the model is run in energy balance mode. ^c Only if run in combination with LISFLOOD-FP. NA: information not available.



2.1 Background

SPHY is a spatially distributed leaky bucket type of model, and is applied on a cell-by-cell basis. The main terrestrial hydrological processes are described in a conceptual way so that changes in storages and fluxes can be assessed adequately over time and space. SPHY is written in the Python programming language using the PCRaster (Karssenberget al. 2001; Karssenberget al. 2010; Karssenberget al. 2002; Schmitz et al. 2009; Schmitz et al. 2013) dynamic modeling framework.

SPHY is grid based and cell values represent averages over a cell (Figure 1). For glaciers, sub-grid variability is taken into account: a cell can be glacier free, partially glacierized, or completely covered by glaciers. The cell fraction not covered by glaciers consists of either land covered with snow or land that is free of snow. Land that is free of snow can consist of vegetation, bare soil, or open water. The dynamic vegetation module accounts for a time-varying fractional vegetation coverage, which affects processes such as interception, effective precipitation, and potential evapotranspiration. Figure 2 provides a schematic overview of the SPHY modeling concepts.

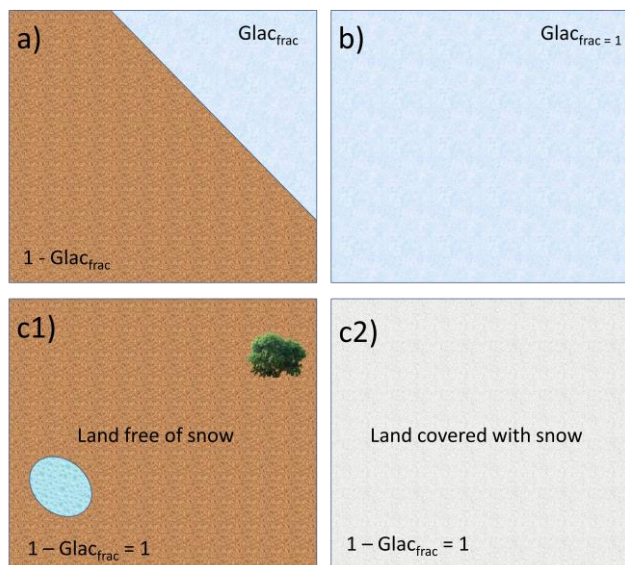


Figure 1: Illustration of SPHY sub-grid variability. A grid cell in SPHY can be (a) partially covered with glaciers, or (b) completely covered with glaciers, or (c1) free of snow, or (c2) completely covered with snow. In the case of (c1), the free land surface can consist of bare soil, vegetation, or open water.



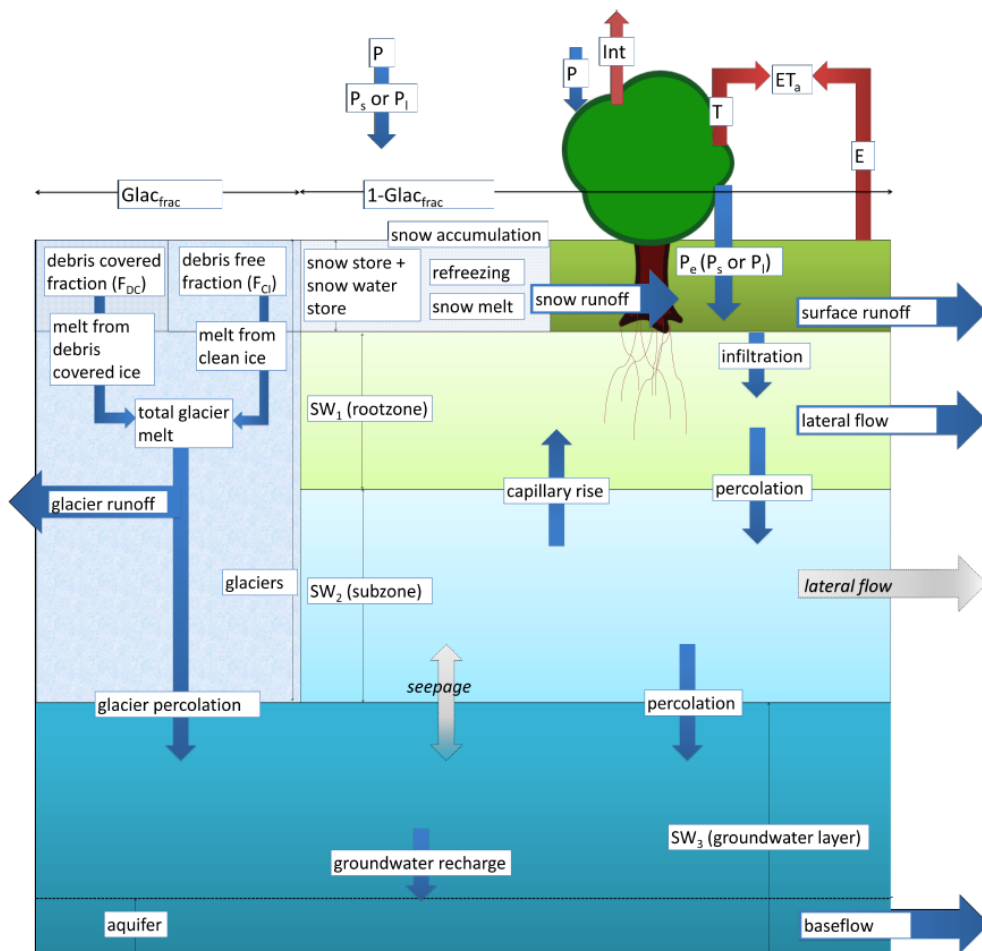


Figure 2: SPHY modeling concepts. The fluxes in grey are only incorporated when the groundwater module is not used. Abbreviations are explained in the text.

The soil column structure is similar to VIC (Liang et al. 1994, 1996), with two upper soil storages and a third groundwater storage. Their corresponding drainage components are surface runoff, lateral flow and baseflow. SPHY simulates for each cell precipitation in the form of rain or snow, depending on the temperature. Precipitation that falls on land surfaces can be intercepted by vegetation and evaporated in part or whole. The snow storage is updated with snow accumulation and/or snowmelt. A part of the liquid precipitation is transformed in surface runoff, whereas the remainder infiltrates into the soil. The resulting soil moisture is subject to evapotranspiration, depending on the soil properties and fractional vegetation cover, while the remainder contributes to river discharge by means of lateral flow from the first soil layer, and baseflow from the groundwater layer.

Melting of glacier ice contributes to the river discharge by means of a slow and fast component, being (i) percolation to the groundwater layer that eventually becomes baseflow, and (ii) direct runoff. The cell-specific runoff, which becomes available for routing, is the sum of surface runoff, lateral flow, baseflow, snowmelt and glacier melt.

If no lakes are present, then the user can choose a simple flow accumulation routing scheme: for each cell, the accumulated amount of water that flows out of the cell into its neighboring downstream cell is calculated. This accumulated amount is the amount of water in the cell itself plus the amount of water in upstream cells of the cell, and is calculated using the flow direction network. If lakes are present, then the fractional accumulation flux routing scheme is used;



depending on the actual lake storage, a fraction of that storage becomes available for routing and is extracted from the lake, while the remaining part becomes the updated actual lake storage. The flux available for routing is routed in the same way as in the simple flow accumulation routing scheme.

As input, SPHY requires static data as well as dynamic data. For the static data, the most relevant are digital elevation model (DEM), land use type, glacier cover, lakes/reservoirs and soil characteristics. The main dynamic data consist of climate data, such as precipitation, temperature, and reference evapotranspiration. Since SPHY is grid based, optimal use of remote sensing data and global data sources can be made. For example, the Normalized Difference Vegetation Index (NDVI) (Tucker 1979; Carlson and Ripley 1997; Myneni and Williams 1994) can be used to determine the leaf-area index (LAI) in order to estimate the growth stage of land cover. For setting up the model, streamflow data are not necessary. However, to undertake a proper calibration and validation procedure, flow data are required. The model could also be calibrated using actual evapotranspiration, soil moisture contents, and/or snow-covered area (SCA). Section 3.2 contains an example application in which the SPHY model has been calibrated using MODIS snow cover images. An overview of the adjustable SPHY model parameters is shown in Appendix 1 (Table 6).

The SPHY model provides a wealth of output variables that can be selected based on the preference of the user. Spatial output can be presented as maps of all the available hydrological processes, i.e., actual evapotranspiration, runoff generation (separated by its components), and groundwater recharge. These maps can be generated on a daily basis, but can also be aggregated at monthly or annual time periods. Time series can be generated for each cell in the study area. Time series often used are streamflow, actual evapotranspiration and recharge to the groundwater.

2.2 Modules

SPHY enables the user to turn on/off modules (processes) that are relevant/irrelevant for the area of interest. This concept is very useful if the user is studying hydrological processes in regions where not all hydrological processes are relevant. A user may for example be interested in studying irrigation water requirements in central Africa. For this region, glacier and snow melting processes are irrelevant, and can thus be switched off. The advantages of turning off irrelevant modules are two-fold: (i) decrease model run time, and (ii) decrease the number of required model input data. It should be noted, however, that the hydrologic model structure should be specific to the catchment's characteristics (Pomeroy et al. 2007; Clark et al. 2008; Niu et al. 2011; Essery et al. 2013; Clark et al., 2015a, 2015b). It is therefore essential that the user knows which catchment characteristics and processes should be included in their modeling framework.

Figure 3 represents an overview of the six modules available: glaciers, snow, groundwater, dynamic vegetation, simple routing, and lake/reservoir routing. All modules can run independently of each other, except for the glacier module. If glaciers are present, then snow processes are relevant as well (Verbunt et al. 2003; Singh and Kumar 1997). Since melting glacier water percolates to the groundwater layer, the glacier module cannot run with the groundwater module turned off. Two modules are available for runoff routing: (i) a simple flow accumulation routing scheme, and (ii) a fractional flow accumulation routing scheme used when lakes/reservoirs are present. The user has the option to turn off routing, or to choose between



one of these two routing modules. All hydrological processes incorporated in the SPHY model are described in detail in the following sections.

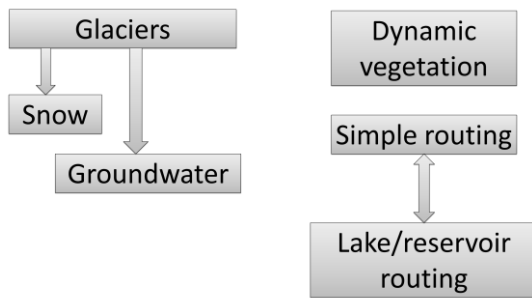


Figure 3: Modules of the SPHY model that can be switched on/off.

2.3 Reference and potential evapotranspiration

Despite the good physical underlying theory of the Penman–Monteith equation (Allen et al. 1998) for calculating the reference evapotranspiration (ET), its major limitation is the high data demand for energy-based methods. This brought Hargreaves and Samani (1985) to derive the modified Hargreaves equation that is based on temperature only. For this reason, this equation has also been implemented in the SPHY model, according to

$$ET_r = 0.0023 \cdot 0.408 \cdot Ra(T_{avg} + 17.8) \cdot TD^{0.5}$$

Equation 1

with Ra ($MJm^{-2}d^{-1}$) the extraterrestrial radiation, T_{avg} (C) the average daily air temperature, and TD (C) the daily temperature range, defined as the difference between the daily maximum and minimum air temperature. The constant 0.408 is required to convert the units to mm, and Ra can be obtained from tables (Allen et al. 1998) or equations using the day of the year and the latitude of the area of interest.

According to Allen et al. (1998), ET_r is the evapotranspiration rate from a reference surface with access to sufficient water to allow evapotranspiration at the potential rate. The reference surface is a hypothetical grass reference crop with specific characteristics. The potential evapotranspiration ET_p has no limitations on crop growth or evapotranspiration from soil water and salinity stress, crop density, pests and diseases, weed infestation or low fertility. Allen et al. (1998) determined ET_p by the crop coefficient approach, where the effects of various weather conditions are incorporated into ET_r and the crop characteristics in the crop coefficient (Kc), using

$$ET_{p,t} = ET_{r,t} \cdot Kc$$

Equation 2

with $ET_{p,t}$ (mm) the potential evapotranspiration on day t , $ET_{r,t}$ (mm) the reference evapotranspiration on day t , and Kc (–) the crop coefficient. The effects of both crop transpiration and soil evaporation are integrated into the Kc .

If the dynamic vegetation module in SPHY is not used, then the user can opt (i) to use a single constant Kc throughout the entire simulation period or (ii) to use a pre-defined time series of crop coefficients as model input. Plausible values for Kc can be obtained from the literature (Allen et al. 1998; FAO 2013). However, vegetation is generally very dynamic throughout the



year. It is therefore more realistic to use a pre-defined time series of crop coefficients or to use the dynamic vegetation module, instead of a single constant K_c . This can be adjusted according to the user's preferences.

K_c can be estimated using remotely sensed data (Rafn et al., 2008; Contreras et al., 2014). In the dynamic vegetation module, K_c is scaled throughout the year using NDVI and the maximum and minimum values for K_c , which are crop specific. These values for K_c can easily be obtained from Allen et al. (1998). Then K_c is calculated using

$$K_c = K_{c_{min}} + (K_{c_{max}} - K_{c_{min}}) * \frac{(NDVI - NDVI_{min})}{(NDVI_{max} - NDVI_{min})}$$

Equation 3

with $NDVI_{max}$ (-) and $NDVI_{min}$ (-) the maximum and minimum values for NDVI (vegetation type dependent). This approach shows the flexibility of SPHY in using remote sensing data (e.g., NDVI) as input to improve model accuracy.

2.4 Dynamic vegetation processes

2.4.1 Maximum canopy storage

SPHY allows the user to use the dynamic vegetation module in order to incorporate a time-variable vegetation cover and corresponding rainfall interception. In order to calculate the rainfall interception, the canopy storage needs to be calculated, using a time series of NDVI (Carlson and Ripley 1997). The first step involves the calculation of the fraction photosynthetically active radiation (FPAR). FPAR can be calculated using a relation between NDVI and FPAR, which was found by Peng et al. (2012) and described by Sellers et al. (1996), according to

$$FPAR = \min \left(\frac{(SR - SR_{min})(FPAR_{max} - FPAR_{min})}{(SR_{max} - SR_{min})} + FPAR_{min}, 0.95 \right)$$

Equation 4

with

$$SR = \frac{1 + NDVI}{1 - NDVI}$$

Equation 5

and $FPAR_{max}$ (-) and $FPAR_{min}$ (-) having values of 0.95 and 0.001, respectively. An FPAR of 0.95 is equivalent to the maximum LAI for a particular class, and an FPAR of 0.001 is equivalent to a minimum LAI. In order to calculate FPAR, an NDVI time series is required.

The second step is the calculation of the leaf-area index (LAI), which is eventually required to calculate the maximum canopy storage ($Scan_{max}$). According to Monteith (1973), LAI for vegetation that is evenly distributed over a surface can be calculated using a logarithmic relation between LAI and FPAR, according to

$$LAI = LAI_{max} \cdot \frac{\log(1 - FPAR)}{\log(1 - FPAR_{max})}$$



with LAI (–) the leaf-area index, and LAI_{max} (–) the maximum leaf-area index (vegetation type dependent). This means that the maximum and minimum LAI values are related to the maximum and minimum of FPAR. Table 2 shows the LAI_{max} values for a certain number of vegetation types.

Table 2: LAI_{max} values for different vegetation types (Sellers et al., 1996).

Vegetation type	LAI_{max} [-]
Broadleaf evergreen trees	7
Broadleaf deciduous trees	7
Mixed trees	7.5
Needleleaf evergreen trees	8
High latitude deciduous trees	8
Grass with 10 - 40% woody cover	5
Grass with <10% woody cover	5
Shrubs and bare soil	5
Moss and lichens	5
Bare	5
Cultivated	6

For vegetation that is concentrated in clusters, the linear relation from Goward and Huemmrich (1992) is often used. However, since SPHY is generally applied using grid-cell resolutions between 250m and 1km, we can assume that the effect of having vegetation concentrated in clusters is negligible. Therefore, the calculation of LAI in SPHY is done using the logarithmic relation of Monteith (1973) (Equation 6).

The next step involves the calculation of the maximum canopy storage ($Scan_{max}$ (mm)). Many different relations between $Scan_{max}$ and LAI can be found in the literature, depending on the vegetation type (Jong and Jetten 2010). The best results for crop canopies are shown by Kozak et al. (2007) and are archived by Von Hoyningen-Huene (1981), who derived the following relation between $Scan_{max}$ and LAI:

$$Scan_{max} = 0.935 + 0.498LAI - 0.00575LAI^2$$

Equation 7

2.4.2 Interception

Interception is calculated on a daily basis if the dynamic vegetation module is used, and consists of the daily precipitation plus the intercepted water remaining in the canopy storage from the previous day. First, the canopy storage is updated with the amount of precipitation of the current day:

$$Scan_t = Scan_{t-1} + P_t$$

Equation 8

with $Scan_t$ (mm) the canopy storage on day t , $Scan_{t-1}$ (mm) the canopy storage on day $t - 1$, and P_t (mm) the amount of precipitation on day t . The portion of precipitation that cannot be stored in the canopy storage is known as precipitation throughfall, or effective precipitation, according to:

$$Pe_t = \max(0, Scan_t - Scan_{max,t})$$

Equation 9



with Pe_t (mm) the effective precipitation on day t , and $Scan_t$ (mm) the canopy storage on day t . This equation shows that precipitation throughfall only occurs if the water stored in the canopy exceeds the maximum canopy storage. After the effective precipitation has been calculated, the canopy storage is updated as:

$$Scan_t = Scan_t - Pe_t \quad \text{Equation 10}$$

The remaining amount of water stored in the canopy is available for interception, and the amount of water that will be intercepted depends on the atmospheric demand for open water evaporation. A commonly used value for the atmospheric demand for open water evaporation is 1.5 (Allen et al. 1998), which is derived from the ratio between 1 and the mean pan evaporation coefficient K_p (~ 0.65). The interception can now be calculated using:

$$Int_t = \min(1.5ET_{r,t}, Scan_t) \quad \text{Equation 11}$$

with Int_t (mm) the intercepted water on day t , and $ET_{r,t}$ (mm) the reference evapotranspiration on day t . Finally, the canopy storage is updated by subtracting the interception:

$$Scan_t = Scan_t - Int_t \quad \text{Equation 12}$$

2.5 Snow processes

For each cell, a dynamic snow storage is simulated at a daily time step, adopted from the model presented by Kokkonen et al. (2006). The model keeps track of a snow storage, which is fed by precipitation and generates runoff from snowmelt. Refreezing of snowmelt and rainfall within the snowpack are simulated as well.

2.5.1 Snow and rainfall

Depending on a temperature threshold, precipitation is defined as falling in either solid or liquid form. Daily snow accumulation, which is defined as solid precipitation, is calculated as:

$$P_{s,t} = \begin{cases} Pe_t & \text{if } T_{avg,t} \leq T_{crit} \\ 0 & \text{if } T_{avg,t} > T_{crit} \end{cases} \quad \text{Equation 13}$$

with $P_{s,t}$ (mm) the snowfall on day t , Pe_t (mm) the effective precipitation on day t , $T_{avg,t}$ ($^{\circ}\text{C}$) the mean air temperature on day t , and T_{crit} ($^{\circ}\text{C}$) a calibrated temperature threshold for precipitation to fall as snow. The precipitation that falls as rain is defined as liquid precipitation, and is calculated as:

$$P_{l,t} = \begin{cases} Pe_t & \text{if } T_{avg,t} > T_{crit} \\ 0 & \text{if } T_{avg,t} \leq T_{crit} \end{cases} \quad \text{Equation 14}$$

with $P_{l,t}$ (mm) being the amount of rainfall on day t .



2.5.2 Snowmelt, refreezing, and storage

To simulate snowmelt, the well-established and widely used degree-day melt modeling approach is used (Hock 2003). The application of degree-day models is widespread in cryospheric models and is based on an empirical relationship between melt and air temperature. Degree-day models are easier to set up compared to energy-balance models, and only require air temperature, which is mostly available and relatively easy to interpolate (Hock 2005). Using a degree-day modeling approach, the daily potential snowmelt is calculated as follows:

$$A_{\text{pot},t} = \begin{cases} T_{\text{avg},t} \cdot \text{DDF}_s & \text{if } T_{\text{avg},t} > 0 \\ 0 & \text{if } T_{\text{avg},t} \leq 0 \end{cases}$$

Equation 15

with $A_{\text{pot},t}$ (mm) the potential snowmelt on day t , and DDF_s ($\text{mm } ^\circ\text{C}^{-1}\text{d}^{-1}$) a calibrated degree-day factor for snow. The actual snowmelt is limited by the snow storage at the end of the previous day, and is calculated as:

$$A_{\text{act},t} = \min(A_{\text{pot},t}, \text{SS}_{t-1})$$

Equation 16

with $A_{\text{act},t}$ (mm) the actual snowmelt on day t , and SS_{t-1} (mm) the snow storage on day $t - 1$. The snow storage from day $t - 1$ is then updated to the current day t , using the actual snowmelt ($A_{\text{act},t}$) and the solid precipitation ($P_{s,t}$). Part of the actual snowmelt freezes within the snowpack and thus does not run off immediately. When temperature is below the melting point, meltwater that has frozen in the snowpack during $t - 1$ is added to the snow storage as:

$$\text{SS}_t = \begin{cases} \text{SS}_{t-1} + P_{s,t} + \text{SSW}_{t-1} & \text{if } T_{\text{avg},t} < 0 \\ \text{SS}_{t-1} + P_{s,t} - A_{\text{act},t} & \text{if } T_{\text{avg},t} \geq 0 \end{cases}$$

Equation 17

with SS_t the snow storage on day t , SS_{t-1} the snow storage on day $t - 1$, $P_{s,t}$ the solid precipitation on day t , $A_{\text{act},t}$ the actual snowmelt on day t , and SSW_{t-1} the amount of frozen meltwater on day $t - 1$. The units for all terms are mm.

The capacity of the snowpack to freeze snowmelt is characterized by introducing a calibrated water storage capacity (SSC ($\text{mm} \cdot \text{mm}^{-1}$)), which is the total water equivalent of snowmelt (mm) that can freeze per mm water equivalent of snow in the snow storage. The maximum of meltwater that can freeze (SSW_{max} (mm)) is thus limited by the thickness of the snow storage:

$$\text{SSW}_{\text{max},t} = \text{SSC} \cdot \text{SS}_t$$

Equation 18

Then the amount of meltwater stored in the snowpack, and that can freeze in the next time step, is calculated as:

$$\text{SSW}_t = \begin{cases} 0, & \text{if } T_{\text{avg},t} < 0 \\ \min(\text{SSW}_{\text{max},t}, \text{SSW}_{t-1} + P_{l,t} + A_{\text{act},t}), & \text{if } T_{\text{avg},t} \geq 0 \end{cases}$$

Equation 19

with SSW_t the amount of meltwater in the snowpack on day t , $\text{SSW}_{\text{max},t}$ the maximum of meltwater that can freeze on day t , SSW_{t-1} the amount of frozen meltwater on day $t - 1$, $P_{l,t}$ the



amount of rainfall on day t , and $A_{act,t}$ the actual snowmelt on day t . The units of all terms are in mm.

The total snow storage (SST (mm)) consists of the snow storage and the meltwater that can freeze within it, according to:

$$SST_t = (SS_t + SSW_t) \cdot (1 - GlacF)$$

Equation 20

with $(1 - GlacF)$ (–) the grid-cell fraction not covered with glaciers. In SPHY it is therefore assumed that snow accumulation and snowmelt can only occur on the grid-cell fraction determined as land surface. Snow falling on glaciers is incorporated in the glacier module.

2.5.3 Snow runoff

Runoff from snow (SRo (mm)) is generated when the air temperature is above melting point and no more meltwater can be frozen within the snowpack, according to:

$$SRo_t = \begin{cases} A_{act,t} + P_{t,t} - \Delta SSW & \text{if } T_{avg,t} > 0 \\ 0 & \text{if } T_{avg,t} \leq 0 \end{cases}$$

Equation 21

with ΔSSW (mm) the change in meltwater stored in the snowpack according to:

$$\Delta SSW = SSW_t - SSW_{t-1}$$

Equation 22

2.6 Glacier processes

Since the SPHY model usually operates at a spatial resolution between 250m and 1km, the dynamics of glaciers such as ice flow cannot be resolved explicitly. Therefore, glaciers in SPHY are considered melting surfaces that can completely or partly cover a grid cell.

2.6.1 Glacier melt

Glacier melt is calculated with a degree-day modeling approach as well (Hock 2005). Because glaciers that are covered with debris melt at different rates than debris-free glaciers (Reid et al. 2012), a distinction can be made between different degree-day factors for both types. The daily melt from debris-free glaciers (A_{CI} (mm)) is calculated as:

$$A_{CI,t} = \begin{cases} T_{avg,t} \cdot DDF_{CI} \cdot F_{CI} & \text{if } T_{avg,t} > 0 \\ 0 & \text{if } T_{avg,t} \leq 0 \end{cases}$$

Equation 23

with DDF_{CI} ($\text{mm } ^\circ\text{C}^{-1}\text{d}^{-1}$) a calibrated degree-day factor for debris-free glaciers and F_{CI} (–) the fraction of debris-free glaciers within the fractional glacier cover ($GlacF$) of a grid cell. The daily melt from debris-covered glaciers (A_{DC} (mm)) is calculated in a similar way, but with a different degree-day factor:



$$A_{DC,t} = \begin{cases} T_{avg,t} \cdot DDF_{DC} \cdot F_{DC} & \text{if } T_{avg,t} > 0 \\ 0 & \text{if } T_{avg,t} \leq 0 \end{cases}$$

Equation 24

where DDF_{DC} ($\text{mm } ^\circ\text{C}^{-1}\text{d}^{-1}$) is a degree-day factor for debris-covered glaciers and F_{DC} (–) is the fraction of debris-covered glaciers within the fractional glacier cover of a grid cell. The total glacier melt per grid cell (A_{GLAC} (mm)) is then calculated by summing the melt from the debris-covered and debris-free glacier types and multiplying by the fractional glacier cover, according to:

$$A_{GLAC,t} = (A_{CI,t} + A_{DC,t}) \cdot \text{GlacF}$$

Equation 25

2.6.2 Glacier runoff

In SPHY, a fraction of the glacier melt percolates to the groundwater while the remaining fraction runs off. The distribution of both is defined by a calibrated glacier melt runoff factor (GlacROF (–)) that can have any value ranging from 0 to 1. Thus, the generated runoff GRO (mm) from glacier melt is defined as:

$$GRO_t = A_{GLAC,t} \cdot \text{GlacROF}$$

Equation 26

2.6.3 Glacier percolation

The percolation from glacier melt to the groundwater (G_{perc} (mm)) is defined as:

$$G_{perc,t} = A_{GLAC,t} \cdot (1 - \text{GlacROF})$$

Equation 27

The percolated glacier water is added to the water that percolates from the soil layers of the non-glacierized part of the grid cell (Section 2.7.1 and 2.7.6), which eventually recharges the groundwater.

2.7 Soil water processes

2.7.1 Soil water balances

The soil water processes in SPHY are modeled for three soil layers (Figure 2), being (i) the first soil layer (root zone), (ii) second soil layer (subzone), and (iii) third soil layer (groundwater layer). The water balance of the first soil layer is:

$$SW_{1,t} = SW_{1,t-1} + Pe_t - ET_{a,t} - RO_t - LF_{1,t} - Perc_{1,t} + Cap_t$$

Equation 28

with $SW_{1,t}$ and $SW_{1,t-1}$ the water content in the first soil layer on days t and $t - 1$, respectively, Pe_t the effective precipitation on day t , $ET_{a,t}$ the actual evapotranspiration on day t , RO_t the surface runoff on day t , $LF_{1,t}$ the lateral flow from the first soil layer on day t , $Perc_{1,t}$ the



percolation from the first to the second soil layer on day t , and Cap_t the capillary rise from the second to the first soil layer on day t . The second soil layer water balance is:

$$SW_{2,t} = SW_{2,t-1} + Perc_{1,t} - Perc_{2,t} - Cap_t$$

Equation 29

with $SW_{2,t}$ and $SW_{2,t-1}$ the water content in the second soil layer on day t and $t - 1$, respectively, and $Perc_{2,t}$ percolation from the second to the third soil layer on day t . The third soil layer water balance is given as:

$$SW_{3,t} = SW_{3,t-1} + Gchrg_t - BF_t$$

Equation 30

with $SW_{3,t}$ and $SW_{3,t-1}$ the water content in the third soil layer on day t and $t - 1$, respectively, $Gchrg_t$ groundwater recharge from the second to the third soil layer on day t , and BF_t baseflow on day t . If the glacier module is used, then groundwater recharge consists of percolation from the second soil layer and percolated glacier melt; otherwise, only percolation from the second soil layer is taken into account.

The user can opt to run SPHY without the third soil layer (groundwater). This may be desirable if the user for example is mainly interested in simulating soil moisture conditions in the root zone, instead of evaluating for instance the contribution of baseflow to the total routed river flow. In that case, only the two upper soil layers are used where the bottom boundary of soil layer two is controlled by a seepage flux (positive outward), and instead of baseflow from the third soil layer, water leaves the second soil layer through lateral flow. With the groundwater module turned off, the water balance for the second soil layer is:

$$SW_{2,t} = SW_{2,t-1} + Perc_{1,t} - LF_{2,t} - Cap_t - Seep$$

Equation 31

with $LF_{2,t}$ lateral flow from the second soil layer, and $Seep$ seepage in or out of the second soil layer (positive is outgoing). The units for all water balance terms are in mm.

2.7.2 Actual evapotranspiration

Evapotranspiration refers to both the transpiration from vegetation and the evaporation from soil or open water. As was mentioned in Section 2.3, the K_c accounts for both the crop transpiration and soil evaporation. The additional use of the dynamic vegetation module accounts for a time-variable vegetation cover, meaning that the role of evaporation becomes more dominant as soon as vegetation cover decreases.

Many limiting factors (e.g., salinity stress, water shortage, water excess, diseases) can cause a reduction in potential evapotranspiration (ET_p), resulting in the actual evapotranspiration rate (ET_a). Since SPHY is a water-balance model, SPHY only accounts for stresses related to water shortage or water excess. If there is too much water in the soil profile, then the plant is unable to extract water because of oxygen stress (Bartholomeus et al. 2008). The calculation of evapotranspiration reduction due to water excess (oxygen stress) is quite complex and requires a substantial number of plant and soil properties (e.g., soil temperature, root dry weight, plant respiration, and minimum gas filled soil porosity; (Bartholomeus et al. 2008)) that are generally not available for the spatial scale that SPHY is applied on. Therefore, SPHY uses an



evapotranspiration reduction parameter ($ET_{red_{wet}}$) that has a value of 0 if the soil is saturated, and otherwise it will have a value of 1. This parameter is used in the following equation to calculate the actual evapotranspiration:

$$ET_{a,t} = ET_{p,t} \cdot ET_{red_{wet}} \cdot ET_{red_{dry}}$$

Equation 32

with $ET_{a,t}$ (mm) the actual evapotranspiration on day t , $ET_{p,t}$ (mm) the potential evapotranspiration on day t , and $ET_{red_{wet}}$ and $ET_{red_{dry}}$ the reduction parameters for water excess and water shortage conditions, respectively. $ET_{red_{dry}}$ is calculated using the Feddes equation (Feddes et al., 1978), which assumes a linear decline in rootwater uptake if the water pressure head drops below a critical value. This critical value can be determined using the soil water retention curve (pF curve), which relates the moisture content of the soil to its binding capacity. This relation is unique for each soil type. The binding capacity is a suction force (H) and is therefore often expressed in cm negative water column. The pF value is simply a conversion of the suction force (H), and is calculated as:

$$pF = \log_{10}(-H)$$

Equation 33

Soils that are at field capacity generally have a pF of 2, meaning -100cm of water column, and soils that are at permanent wilting point have a pF of 4.2, or -16000cm of water column. The permanent wilting point is often referred to as the point where the crop dies. In SPHY it is assumed that the linear decline in rootwater uptake starts at a pF of 3 (-1000cm water column). Therefore, $ET_{red_{dry}}(-)$ is calculated as:

$$ET_{red_{dry,t}} = \frac{SW_{1,t} - SW_{1,pF4.2}}{SW_{1,pF3} - SW_{1,pF4.2}}$$

Equation 34

with $ET_{red_{dry,t}}(-)$ the reduction in rootwater uptake due to water shortage on day t , $SW_{1,t}$ (mm) the actual soil water content in the first soil layer on day t , and $SW_{1,pF3}$ (mm) and $SW_{1,pF4.2}$ (mm) the soil water content in the first soil layer at pF3 and pF4.2, respectively. $ET_{red_{dry}}$ can therefore have values ranging between 0 and 1, where a value of 1 represents optimal plant growing conditions, and 0 means no rootwater uptake at all. $ET_{red_{dry}}$ is eventually used in Equation 32 to calculate the ET_a .

2.7.3 Surface runoff

Since the SPHY model runs on a daily time step, the model does not account for sub-daily variability in rainfall intensities. Therefore, the Hortonian runoff process (Beven 2004; Corradini et al., 1998), which refers to infiltration excess overland flow, is considered less important. For this reason, SPHY uses the saturation excess overland flow process, known as Hewlettian runoff (Hewlett 1961), to calculate surface runoff. Surface runoff is calculated from the first soil layer:

$$RO = \begin{cases} SW_1 - SW_{1,sat} & \text{if } SW_1 > SW_{1,sat} \\ 0 & \text{if } SW_1 \leq SW_{1,sat} \end{cases}$$

Equation 35



with RO (mm) surface runoff, SW_1 (mm) the water content in the first soil layer, and $SW_{1,sat}$ (mm) the saturated water content of the first soil layer.

2.7.4 Lateral flow

Lateral flow is substantial in catchments with steep gradients and soils with high hydraulic conductivities (Beven 1981; Beven and Germann 1982; Sloan and Moore 1984). In SPHY, it is assumed that only the amount of water exceeding field capacity can be used for lateral flow. Therefore, the drainable volume of water (excess water) needs to be calculated first:

$$W_{l,exc} = \begin{cases} SW_l - SW_{l,fc} & \text{if } SW_l > SW_{l,fc} \\ 0 & \text{if } SW_l \leq SW_{l,fc} \end{cases}$$

Equation 36

with $W_{l,exc}$ (mm) the drainable volume of water from soil layer l , SW_l (mm) the water content in soil layer l , and $SW_{l,fc}$ (mm) the field capacity of soil layer l . According to Sloan and Moore (1984), the lateral flow at the hillslope outlet can be calculated as:

$$LF_l^* = W_{l,excfrac} \cdot v_{lat,l}$$

Equation 37

with LF_l^* (mm) lateral flow from soil layer l , $W_{l,excfrac}$ (–) the drainable volume of water as a fraction of the saturated volume, and $v_{lat,l}$ ($\text{mm} \cdot \text{d}^{-1}$) the flow velocity at the outlet. In SPHY, the drainable volume as a fraction of the saturated volume is calculated as:

$$W_{l,excfrac} = \frac{W_{l,exc}}{SW_{l,sat} - SW_{l,fc}}$$

Equation 38

The velocity of flow at the outlet, $v_{lat,l}$ ($\text{mm} \cdot \text{d}^{-1}$), depends on both the saturated hydraulic conductivity $K_{sat,l}$ ($\text{mm} \cdot \text{d}^{-1}$) and the slope of the hill slp (–), and is defined as:

$$v_{lat,l} = K_{sat,l} \cdot \text{slp}$$

Equation 39

The slope (slp) in SPHY is calculated for each grid cell as the increase in elevation per unit distance.

According to Neitsch et al. (2009), only a fraction of lateral flow will reach the main channel on the day it is generated if the catchment of interest has a time of concentration greater than 1 day. This concept is also implemented in the SPHY model, and uses a lateral flow travel time $TT_{lag,l}$ (d) to lag a portion of lateral flow release to the channel:

$$LF_l = (LF_l^* + LF_{l,t-1}^*) \cdot \left(1 - \exp \left[\frac{-1}{TT_{lag,l}} \right] \right)$$

Equation 40

with LF_l (mm) the amount of lateral flow entering the channel on a given day, LF_l^* (mm) the lateral flow (Equation 37) generated within the cell on a given day, and $LF_{l,t-1}^*$ (mm) the lateral flow lagged from the previous day. SPHY assumes the lateral flow travel time to be dependent



on the field capacity $SW_{l,fc}$ (mm), saturated content $SW_{l,sat}$ (mm), and the saturated conductivity $K_{sat,l}$ ($\text{mm} \cdot \text{d}^{-1}$), according to:

$$TT_{lag,l} = \frac{SW_{l,sat} - SW_{l,fc}}{K_{sat,l}}$$

Equation 41

A longer lateral flow travel time will result in a smoother streamflow hydrograph.

2.7.5 Percolation

If the groundwater module is used, then water can percolate from the first to the second soil layer, and from the second to the third soil layer. If the user decides to run SPHY without the groundwater module, percolation only occurs from the first to the second soil layer. In SPHY, water can only percolate if the water content exceeds the field capacity of that layer, and the water content of the underlying layer is not saturated. A similar approach has been used in the SWAT model (Neitsch et al. 2009). The water volume available for percolation to the underlying layer is calculated as:

$$W_{l,exc} = \begin{cases} 0, & \text{if } SW_l \leq SW_{l,fc} \text{ or } SW_{l+1} \geq SW_{l+1,sat} \\ SW_{l+1,sat} - SW_{l+1}, & \text{if } SW_l - SW_{l,fc} > SW_{l+1,sat} - SW_{l+1} \\ SW_l - SW_{l,fc}, & \text{else} \end{cases}$$

Equation 42

with $W_{l,exc}$ (mm) the drainable volume of water from layer l , SW_l (mm) the water content in layer l , $SW_{l,fc}$ (mm) the field capacity of layer l , SW_{l+1} (mm) the water content in layer $l + 1$, and $SW_{l+1,sat}$ (mm) the saturated water content of layer $l + 1$. Only a certain amount of $W_{l,exc}$ will percolate to the underlying soil layer, depending on the percolation travel time $TT_{perc,l}$ (d). This approach follows the storage routing methodology, which is also implemented in the SWAT model (Neitsch et al. 2009):

$$w_{l,perc} = W_{l,exc} \cdot \left(1 - \exp \left[\frac{-1}{TT_{perc,l}} \right] \right)$$

Equation 43

with $w_{l,perc}$ (mm) the amount of water percolating to the underlying soil layer. Since the speed at which water can move through the soil is mainly dependent on the saturated hydraulic conductivity (K_{sat}), the travel time for percolation is calculated the same way as the travel time for lateral flow (Equation 41).

2.7.6 Groundwater recharge

Water that percolates from the second to the third soil layer will eventually reach the shallow aquifer. This process is referred to as groundwater recharge hereafter. If the glacier module is used as well, then glacier melt that percolates also contributes to the groundwater recharge. Groundwater recharge often does not occur instantaneously, but with a time lag that depends on the depth of the groundwater table and soil characteristics. SPHY uses the same exponential decay weighting function as proposed by Venetis (1969) and used by Sangrey, Harrop-Williams, and Klaiber (1984) in a precipitation groundwater response model. This approach has also been adopted in the SWAT model (Neitsch et al. 2009), using:



$$Gchrg_t = \left(1 - \exp\frac{-1}{\delta_{gw}}\right) \cdot w_{2,perc} + \exp\frac{-1}{\delta_{gw}} \cdot Gchrg_{t-1}$$

Equation 44

with $Gchrg_t$ (mm) and $Gchrg_{t-1}$ (mm) the groundwater recharge on days t and $t - 1$, respectively. δ_{gw} (d) is the delay time and $w_{2,perc}$ (mm) is the amount of water that percolates from the second to the third layer on day t .

2.7.7 Baseflow

After groundwater recharge has been calculated, SPHY calculates baseflow, which is defined as the flow going from the shallow aquifer to the main channel. Baseflow only occurs when the amount of water stored in the third soil layer exceeds a certain threshold (BF_{thresh}) that can be specified by the user. Baseflow calculation in SPHY is based on the steady-state response of groundwater flow to recharge (Hooghoudt 1940) and the water table fluctuations that are a result of the non-steady response of groundwater flow to periodic groundwater recharge (Smedema and Rycroft 1983). The SWAT model (Neitsch et al. 2009) assumes a linear relation between the variation in groundwater flow (baseflow) and the rate of change in water table height, according to:

$$\frac{dBF}{dt} = 10 \cdot \frac{K_{sat}}{\mu L_{gw}^2} \cdot (Gchrg - BF) = \alpha_{gw} \cdot (Gchrg - BF)$$

Equation 45

with BF (mm) the groundwater flow (baseflow) into the main channel on day t , K_{sat} (mm d^{-1}) the hydraulic conductivity of the shallow aquifer, μ (–) the specific yield of the shallow aquifer, L_{gw} (m) the distance from the subbasin divide for the groundwater system to the main channel, $Gchrg$ (mm) the amount of groundwater (Equation 44) recharge entering the shallow aquifer on day t , and α_{gw} (–) the baseflow recession coefficient. Equation 45 can be integrated and rearranged to calculate baseflow, according to:

$$BF_t = \begin{cases} 0, & \text{if } SW_3 \leq BF_{thresh} \\ BF_{t-1} \cdot \exp^{-\alpha_{gw}} + Gchrg_t \cdot (1 - \exp^{-\alpha_{gw}}), & \text{if } SW_3 > BF_{thresh} \end{cases}$$

Equation 46

with BF_t (mm) the baseflow into the channel on day t , and BF_{t-1} (mm) the baseflow into the channel on day $t - 1$. Since this equation has proven its success in the SWAT model (Neitsch et al. 2009) throughout many applications worldwide, this equation has been adopted in the SPHY model as well.

The baseflow recession coefficient (α_{gw}) is an index that relates the baseflow response to changes in groundwater recharge. Lower values for α_{gw} therefore correspond to areas that respond slowly to groundwater recharge, whereas higher values indicate areas that have a rapid response to groundwater recharge. The baseflow recession coefficient is generally used as a calibration parameter in the SPHY model, but a good first approximation of this coefficient can be calculated using the number of baseflow days (Neitsch et al. 2009):

$$\alpha_{gw} = \frac{2.3}{BFD}$$

Equation 47



with BFD (d) the number of baseflow days, which is defined as the number of days required for baseflow recession to decline.

2.8 Routing

After calculating the different runoff components, the cell-specific total runoff (Q_{Tot}) is calculated by adding these different runoff components. Depending on the modules being switched on, the different runoff components are i) rainfall runoff (RRo), (ii) snow runoff (SRo), (iii) glacier runoff (GRo), and iv) baseflow (BF). Rainfall runoff is the sum of surface runoff (RO, Section 2.7.3) and lateral flow from the first soil layer (LF_1 , Section 2.7.4). If the groundwater module is not used, then baseflow is calculated as being the lateral flow from the second soil layer. Q_{Tot} is eventually calculated according to:

$$Q_{Tot} = RRo + SRo + GRo + BF$$

Equation 48

with Q_{Tot} (mm) the cell-specific total runoff, RRo (mm) rainfall runoff, SRo (mm) snow runoff, GRo (mm) glacier runoff, and BF (mm) baseflow from the third soil layer or lateral flow from the second soil layer. In order to obtain river discharge, Q_{Tot} needs to be routed through a flow direction network. SPHY allows the user to opt between the use of a simple routing scheme (Section 2.8.1) or a more complex routing scheme (Section 2.8.2) that involves the calculation of lake outflow through $Q(h)$ relations. Both methods require a flow direction network map, which can be obtained by delineating a river network using PCRaster or GIS software in combination with a digital elevation model (DEM).

2.8.1 Runoff routing

In hydrology, streamflow routing is referred to as the transport of water through an open-channel network. Since open-channel flow is unsteady, streamflow routing often involves solving complex partial differential equations. The St. Venant equations (Brutsaert 1971; Morris and Woolhiser 1980) are often used for this, but these have high data requirements related to the river geometry and morphology, which are unavailable for the spatial scale SPHY is generally applied on. Additionally, solving these equations requires the use of very small time steps, which result in large model calculation times. The use of very small time steps in the St. Venant equations is required to provide numerical stability. Other models, such as, e.g., SWAT (Neitsch et al. 2009), use the Manning equation (Manning 1989) to define the rate and velocity of river flow in combination with the variable storage (Williams 1975) or Muskingum (Gill 1978) routing methods to obtain river streamflow. But, the Manning equation also requires river bed dimensions, which are generally unknown on the spatial scale that SPHY generally is applied on.

Therefore, SPHY calculates for each cell the accumulated amount of water that flows out of the cell into its neighboring downstream cell. This can easily be obtained by using the *accflux* PCRaster built-in function, which calculates for each cell the accumulated specific runoff from its upstream cells, including the specific runoff generated within the cell itself. If only the *accflux* function is used, then it is assumed that all the specific runoff generated within the catchment on one day will end up at the most downstream location within one day, which is not plausible. Therefore, SPHY implements a flow recession coefficient (k_x (-)) that accounts for flow delay, which can be a result of channel friction. Using this coefficient, river flow in SPHY is calculated using the three equations shown below:



$$QTot_t^* = \frac{QTot_t \cdot 0.001 \cdot A}{24 \cdot 3600}$$

Equation 49

$$Q_{accu,t} = \text{accuflux}(F_{dir}, QTot_t^*)$$

Equation 50

$$Q_{rout,t} = (1 - kx) \cdot Q_{accu,t} + kx \cdot Q_{rout,t-1}$$

Equation 51

with $QTot_t^*$ (m^3s^{-1}) the specific runoff on day t , $QTot_t$ the specific runoff in mm on day t , A (m^2) the grid-cell area, $Q_{accu,t}$ (m^3s^{-1}) the accumulated streamflow on day t without flow delay taken into account, $Q_{rout,t}$ (m^3s^{-1}) the routed streamflow on day t , $Q_{rout,t-1}$ (m^3s^{-1}) the routed streamflow on day $t - 1$, F_{dir} the flow direction network, and kx (–) the flow recession coefficient kx has values ranging between 0 and 1, where values close to 0 correspond to a fast responding catchment, and values approaching 1 correspond to a slow responding catchment.

The user can opt to route each of the four streamflow contributors separately, which may be useful if one wants to evaluate, for example, the contribution of glacier melt or snowmelt to the total routed runoff. However, this increases model run time substantially, because the accuflux function, which is a time-consuming function, needs to be called multiple times, depending on the number of flow contributors to be routed.

2.8.2 Lake/reservoir routing

Lakes or reservoirs act as a natural buffer, resulting in a delayed release of water from these water bodies. SPHY allows the user to choose a more complex routing scheme if lakes/reservoirs are located in their basin of interest. The use of this more advanced routing scheme requires a known relation between lake outflow and lake level height ($Q(h)$ relation) or lake storage.

To use this routing scheme, SPHY requires a nominal map with the lake cells having a unique ID, and the non-lake cells having a value of 0. The user can supply a Boolean map with “True” for cells that have measured lake levels, and “False” for lake cells that do not have measured lake levels. This specific application of SPHY is discussed in detail in Section 3.3.

Four different relations can be chosen to calculate the lake outflow from the lake level height or lake storage, being (i) an exponential relation, (ii) a first-order polynomial function, (iii) a second-order polynomial function, and (iv) a third-order polynomial function. The user needs to supply maps containing the coefficients used in the different functions.

The lake/reservoir routing scheme simply keeps track of the actual lake storage, meaning that an initial lake storage should be supplied. Instead of the simple accuflux function described in the previous section, the lake/reservoir routing scheme uses the PCRaster functions `accufractionstate` and `accufractionflux`. The `accufractionflux` calculates for each cell the amount of water that is transported out of the cell, while the `accufractionstate` calculates the amount of water that remains stored in the cell. For non-lake cells, the fraction that is transported to the next cell is always equal to 1, while the fraction that is transported out of a lake/reservoir cell depends on the actual lake storage. Each model time step, the lake storage is updated by inflow from upstream. Using this updated storage, the lake level and corresponding lake outflow can



be calculated using one of the four relations mentioned before. The lake outflow can then be calculated as a fraction (Q_{frac} (-)) of the actual lake storage. Instead of using Equation 50, Q_{frac} is then used in Equation 52 and Equation 53 to calculate the accumulated streamflow and updated storage, respectively:

$$Q_{accu,t} = \text{accufractionflux}(F_{dir}, S_{act,t}, Q_{frac,t}) \quad \text{Equation 52}$$

$$S_{act,t+1} = \text{accufractionstate}(F_{dir}, S_{act,t}, Q_{frac,t}) \quad \text{Equation 53}$$

with $S_{act,t}$ (m^3) and $S_{act,t+1}$ (m^3) the actual storage and updated storage to be used in the next time step, respectively, and $Q_{accu,t}$ ($m^3 d^{-1}$) the accumulated streamflow on day t , without flow delay taken into account. Since Q_{frac} is always equal to 1 for the non-lake cells, the accufractionflux function becomes equal to the accuflux function used in the previous section. This actually means that for the river network, the same routing function from Section 2.8.1 is used, and that Equation 52 and Equation 53 only apply to lake/reservoir cells.

In order to account for non-linearity and slower responding catchments, the same kx coefficient is used again. This involves applying Equation 51 as a last step after Equation 52 and converting the units from $m^3 d^{-1}$ to $m^3 s^{-1}$. Since the accufractionflux and accufraction state functions are more complex to compute, the use of these functions increases model run time.



3 Applications

The SPHY model has been applied and tested in various studies, including real-time soil moisture predictions in lowlands, operational reservoir inflow forecasting in mountainous catchments, irrigation scenarios in the Nile basin, and climate change impact studies in the snow–glacier–rain dominated Himalayan region. Some example applications will be summarized in the following sections.

3.1 Irrigation management in lowland areas

As SPHY produces spatial outputs for the soil moisture content in the root zone and the potential and actual evapotranspiration (ET), it is a useful tool for application in agricultural water management decision support. By facilitating easy integration of remote sensing data, crop growth stages can be spatially assessed at different moments in time. The SPHY dynamic vegetation module ensures that all relevant soil water fluxes correspond to crop development stages throughout the growing season. Spatially distributed maps of root water content and ET deficit can be produced, enabling both the identification of locations where irrigation is required and a quantitative assessment of crop water stress.

SPHY has been applied with the purpose of providing field-specific irrigation advice for a large-scale farm in western Romania, comprising 380 individual fields and approximately ten different crops. Contrary to the other case studies highlighted in this paper, a high spatial resolution is very relevant for supporting decisions on variable-rate irrigation. The model has therefore been set up using a 30m resolution, covering the 2013 and 2014 cropping seasons on a daily time step. Optical satellite data from Landsat 8 (USGS 2013) were used as input to the dynamic vegetation module. Soil properties were derived from the Harmonized World Soil Database (Batjes et al. 2012), which for Romania contains data from the Soil Geographical Database for Europe (Lambert et al. 2003). Using the Van Genuchten equation (Van Genuchten 1980), soil saturated water content, field capacity, and wilting point were determined for the HWSD classes occurring at the study site. Elevation data was obtained from the EU-DEM data set (EEA 2014), and air temperature was measured by two on-farm weather stations.

In irrigation management applications like these, a model should be capable of simulating the moisture stress experienced by the crop due to insufficient soil moisture contents, which manifests itself by an evapotranspiration deficit (potential ET – actual ET > 0). Figure 4 shows the spatial distribution of ET deficit, as simulated by the SPHY model for the entire farm on 03 April 2014. When SPHY is run in an operational setting, this spatial information can be included in a decision support system that aids the farmer in irrigation planning for the coming days.



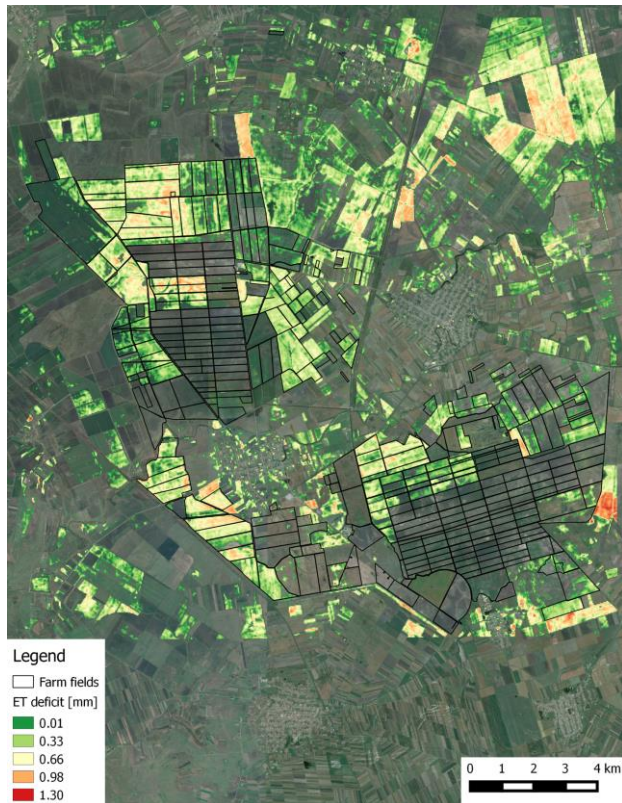


Figure 4: Spatial distribution of evapotranspiration (ET) deficit, as simulated by the SPHY model for a Romanian farm on 03 April 2014. Transparency means no ET deficit.

For calibration purposes, field measurements of soil moisture and/or actual ET are desired. In this case study, one capacitance soil moisture sensor was installed in a soybean field to monitor root-zone water content shortly after 01 May 2014, which is the start of the soybean growing season. The sensor measures volumetric moisture content for every 10cm of the soil profile up to a depth of 60cm. It is also equipped with a rain gauge measuring the sum of rainfall and applied irrigation water, which was used as an input to SPHY. Soil moisture measured over the extent covered by the crop root depth was averaged and compared to simulated values (Figure 5).

Since this study was a demonstration project, only an initial model calibration was performed. The model was in this case most sensitive for the crop coefficient (K_c), affecting the evaporative demand for water. As can be seen in Figure 5, the temporal patterns as measured by the soil moisture sensor are well simulated by the SPHY model. Based on daily soil moisture values, a Nash–Sutcliffe (Nash and Sutcliffe 1970) model efficiency coefficient of 0.6 was found, indicating that the quality of prediction of the SPHY model is “good” (Foglia et al. 2009). Soil moisture simulations could be further improved by conducting a full model calibration, adjusting the soil physical parameters $K_{sat,1}$, $SW_{1,fc}$, $SW_{1,pF3}$, and $SW_{1,pF4.2}$. Remotely sensed evapotranspiration can be used in the calibration process (Immerzeel and Droogers 2008), although such data are often not available on these small scales as ET is a very complex variable to assess (Samain et al. 2012). It should also be noted that soil moisture content is typically highly variable in space; a very high correlation between point measurements and grid-cell simulations of soil moisture may therefore not always be feasible (Bramer et al., 2013).

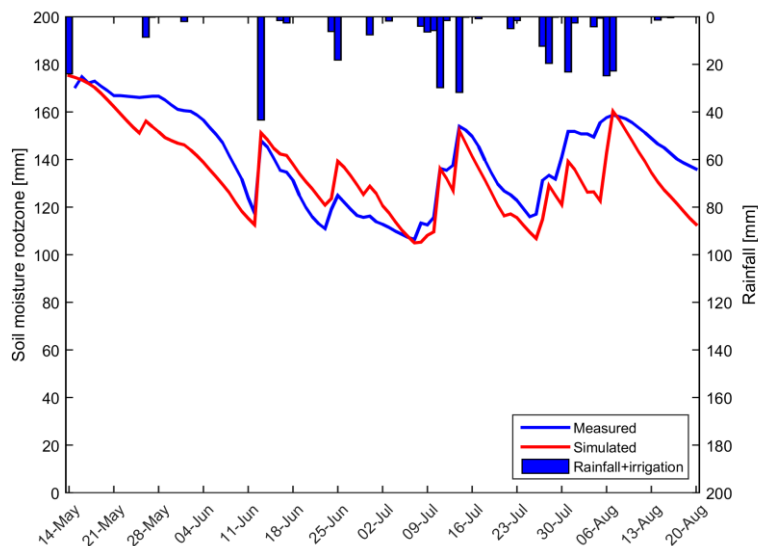


Figure 5: Measured and simulated daily root-zone soil moisture content during the 2014 growing season. Rainfall+irrigation has been measured by the rain gauge that was attached to the moisture sensor.

3.2 Snow- and glacier-fed river basins

SPHY is being used in large Asian river basins with significant contribution of glacier melt and snowmelt to the total flow (Immerzeel et al., 2012, Lutz et al., 2012, 2014a). The major goals of these applications are two-fold:

- Assess the current hydrological regimes at high resolution; e.g., assess spatial differences in the contributions of glacier melt, snowmelt and rainfall–runoff to the total flow.
- Quantify the effects of climate change on the hydrological regimes in the future and how these affect the water availability.

Rivers originating in the high mountains of Asia are considered to be the most meltwater-dependent river systems on Earth (Schaner et al. 2012). In the regions surrounding the Himalayas and the Tibetan Plateau, large human populations depend on the water supplied by these rivers (Immerzeel et al., 2010). However, the dependency on meltwater differs strongly between river basins as a result of differences in climate and differences in basin hypsometry (Immerzeel and Bierkens 2012). Only by using a distributed hydrological modeling approach that includes the simulation of key hydrological and cryospheric processes, and inclusion of transient changes in climate, snow cover, glaciers and runoff, can appropriate adaptation and mitigation options be developed for this region (Sorg et al. 2012). The SPHY model is very suitable for such goals, and has therefore been widely applied in the region.

For application in this region, SPHY was set up at a 1km spatial resolution using a daily time step, and forced with historical air temperature (T_{avg} , T_{max} , T_{min}) and precipitation data, obtained from global and regional data sets (e.g., APHRODITE, (Yatagai et al. 2012); Princeton, (Sheffield, Goteti, and Wood 2006); TRMM, (Gopalan et al. 2010)) or interpolated WMO station data from a historical reference period. For this historical reference period, SPHY was calibrated and validated using observed streamflow. For the future period, SPHY was forced with downscaled climate change projections obtained from general circulation models (GCMs), as



available through the Climate Model Intercomparison Projects (e.g., CMIP3, (Meehl et al. 2007); CMIP5, (Taylor et al., 2012)), which were used as a basis for the Assessment Reports prepared by the Intergovernmental Panel on Climate Change (IPCC).

In central Asia, SPHY was applied in a study (ADB 2012; Immerzeel et al., 2012; Lutz et al., 2012) that focused on the impacts of climate change on water resources in the Amu Darya and Syr Darya river basins. SPHY was used to quantify the hydrological regimes in both basins, and subsequently to project the outflow from the upstream basins to the downstream areas by forcing the model with an ensemble of five CMIP3 GCMs. The SPHY model output fed into a water allocation model that was set up for the downstream parts of the Amu Darya and Syr Darya river basins.

In the Himalayan Climate Change Adaptation Programme (HICAP), led by the International Centre for Integrated Mountain Development (ICIMOD), SPHY has been successfully applied in the upstream basins of the Indus, Ganges, Brahmaputra, Salween and Mekong rivers (Lutz et al. 2013; Lutz et al. 2014a). In this study the hydrological regimes of these five basins have been quantified and the calibrated and validated model (Figure 6) was forced with an ensemble of eight GCMs to create water availability scenarios until 2050. Table 3 lists the calibration and validation results. Based on the validation results, we concluded that the model performs satisfactorily given the large scale, complexity and heterogeneity of the modeled region and data scarcity (Lutz et al. 2014a). We use one parameter set for the entire domain, which inherently means some stations perform better than others. In the particular case of the upper Indus, another possible explanation could be uncertainty in air temperature forcing in the highest parts of the upper Indus basin (locations Dainyor bridge, Besham Qila and Tabela inflow in Table 3), since especially in this area, the used forcing data sets are based on very sparse observations. SPHY allowed the assessment of the current contribution of glacier melt and snowmelt to total flow (Figure 7), and how total flow volumes and the intra-annual distribution of river flow will change in the future (Lutz et al. 2014a).

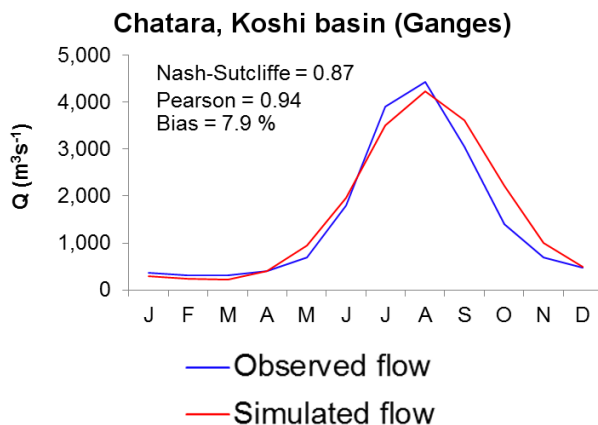


Figure 6: Average monthly observed and SPHY-simulated flow (1998–2007) for the Chatara major discharge measurement location in the Ganges basin (Lutz et al. 2014a). Metrics are calculated based on monthly time steps.



Table 3: Station locations used for calibration and validation of the SPHY model in HICAP (Lutz et al., 2014a). Three stations were used for calibration for 1998–2007. Five stations were used for an independent validation for the same period. The Nash–Sutcliffe efficiency (NS) and bias metrics were calculated at a monthly time step.

Location	NS (–)	Bias (%)	Validation/calibration
Dainyor bridge	0.39	58.2	Validation
Besham Qila	0.66	24.7	Validation
Tarbela inflow	0.63	34.6	Calibration
Marala inflow	0.65	12.0	Validation
Pachuwarghat	0.90	–1.6	Validation
Rabuwa Bazar	0.65	–22.5	Validation
Turkeghat	0.87	–5.4	Calibration
Chatara	0.87	7.9	Calibration

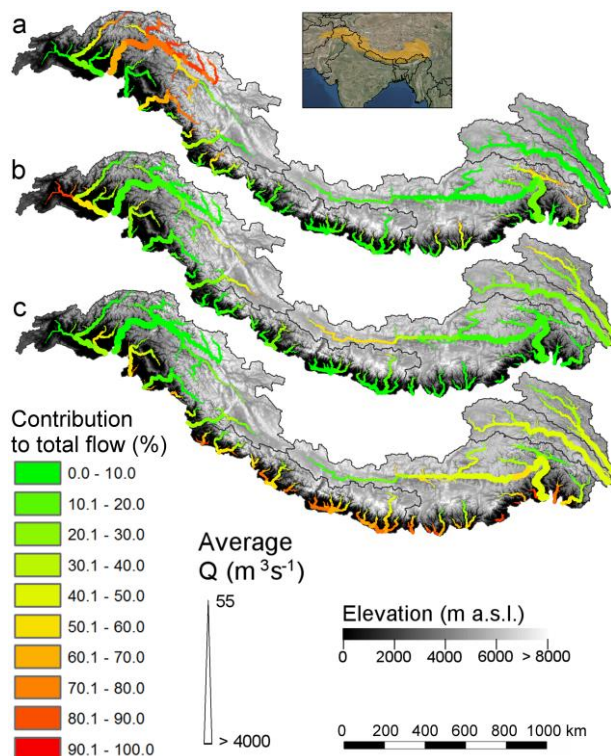


Figure 7: The contribution of glacier melt (a), snowmelt (b), and rainfall (c) to the total flow for major streams in the upstream basins of the Indus, Ganges, Brahmaputra, Salween and Mekong during 1998–2007 (Lutz et al. 2014a).

For basins with snowmelt being an important contributor to the flow, besides calibration to observed flow, the snow-related parameters in the SPHY model can also be calibrated to observed snow cover. For the Upper Indus basin, the snow-related parameters degree-day factor for snow (DDF_s) and snow water storage capacity (SSC) were calibrated independently using MODIS snow cover imagery (Lutz et al., 2014b). The same MODIS data set was used as in Immerzeel et al. (2009). From the beginning of 2000 until halfway through 2008, the snow cover imagery was averaged for 46 different periods of 8 days (5 days for the last period) to generate 46 different average snow cover maps. For example, period 1 is the average snow cover for 01–08 January for 2000 until 2008, whereas period 2 is the average snow cover for 09–16 January for 2000 until 2008, etc. The SPHY model was run for 2000–2007 at a daily time



step and, for each $1 \times 1\text{ km}$ grid cell, the average snow cover was calculated for the same 46 periods as in the MODIS observed snow cover data set. Subsequently, these simulated snow cover maps were resampled to 0.05 spatial resolution, which is the native resolution of the MODIS product. Figure 8 shows the basin-average observed and simulated fractional snow cover for the 46 periods during 2000–2007 and Figure 9 shows the same at the 0.05 grid-cell level. As a final step, the baseflow recession coefficient (α_{gw}) and routing coefficient (k_x) were calibrated to match the simulated streamflow with the observed streamflow.

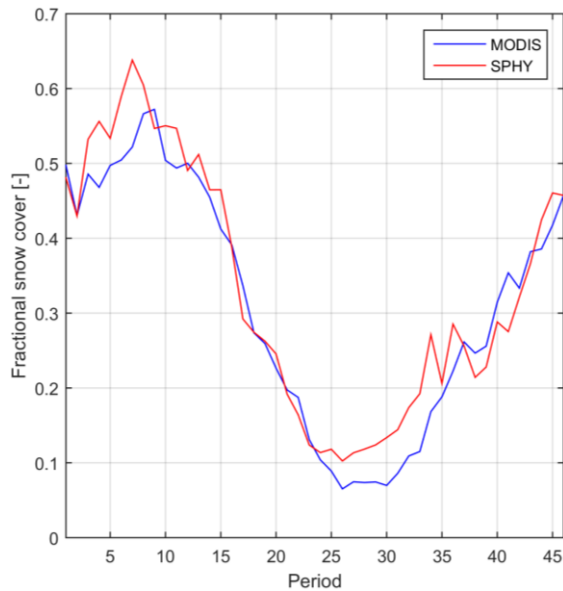


Figure 8: Observed and simulated average fractional snow cover in the upper Indus basin. The values represent the 9-year average for 46 (8-day) periods during 2000–2007.

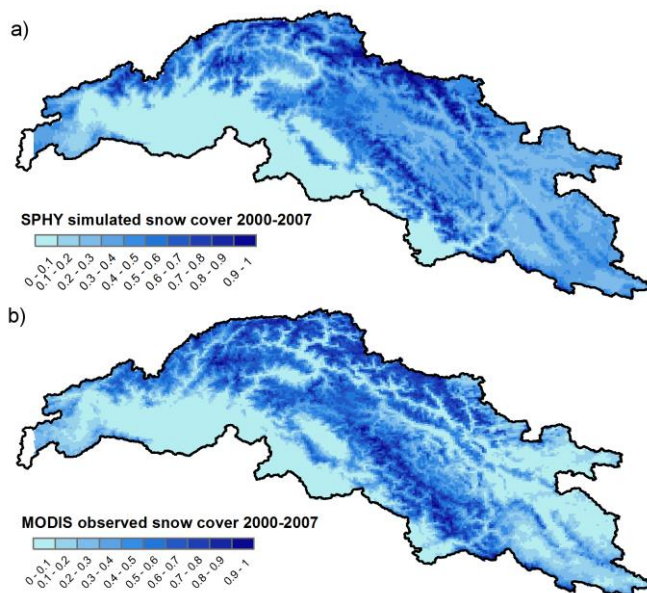


Figure 9: (a) SPHY simulated snow cover 2000–2007 and (b) MODIS observed snow cover 2000–2007.

3.3 Flow forecasting

In data-scarce environments and inaccessible mountainous terrain, like in the Chilean Andes, it is often difficult to install instrumentation and retrieve real-time physical data from these instruments. These real-time data can be useful to capture the hydroclimatic variability in this region, and improve the forecasting capability of hydrological models. Although statistical models can provide skillful seasonal forecasts, using large-scale climate variables and in situ data (Piechota and Chiew 1998; Grantz et al. 2005; Regonda et al. 2006; Bracken et al., 2010), a particular hydropower company in Chile was mainly interested in the potential use of an integrated system, using measurements derived from both Earth observation (EO) satellites and in situ sensors, to force a hydrological model to forecast seasonal streamflow during the snow melting season. The objective of the INTOGENER (INTegration of EO data and GNSS-R signals for ENERgy applications) project was therefore to demonstrate the operational forecasting capability of the SPHY model in data-scarce environments with large hydroclimatic variability.

During INTOGENER, data retrieved from EO satellites consisted of a DEM and a time series of snow cover maps. Snow cover images were retrieved on a weekly basis, using RADARSAT and MODIS (Parajka and Blöschl 2008; Hall et al. 2002) imagery. These images were used to update the snow storage (SS (mm)) in the model in order to initialize it for the forecasting period. Figure 10 shows the snow storage as simulated by the SPHY model during the snow melting season in the Laja basin. These maps clearly show the capability of SPHY to simulate the spatial variation of snow storage, with more snow on the higher elevations, and a decrease in snow storage throughout the melting season. Discharge, precipitation and temperature data were collected using in situ meteorological stations. In order to calculate the lake outflow accurately, the SPHY model was initialized with water level measurements retrieved from reflected Global Navigation Satellite System (GNSS) signals in Laja Lake. Static data that were used in the SPHY model consisted of soil characteristics derived from the Harmonized World Soil Database (HWSD) (Batjes et al. 2009) and land use data obtained from the GLOBCOVER (Bontemps et al. 2011) product. The SPHY model was set up to run at a spatial resolution of 200m.

Figure 11 shows the observed vs. simulated daily streamflow for two locations within the Laja River basin for the historical period 2007–2008. It can be seen that model performance is quite satisfactory for both locations, with volume errors of -4 and -9.4% for the Abanico Canal (downstream of Lake Laja) and Rio Laja en Tucapel, respectively. The NS coefficient, which is especially useful for assessing the simulation of high discharge peaks, is less satisfactory for these locations. Hydropower companies, however, have more interest in expected flow volumes for the coming weeks/months than in accurate day-to-day flow simulations, and therefore the NS coefficient is less important in this case. If the NS coefficient is calculated for the same period on a monthly basis, then the NS coefficients are 0.53 for the Abanico Canal and 0.81 for Rio Laja en Tucapel. It is likely that SPHY model performance would even have been better if a full model calibration would have been performed.



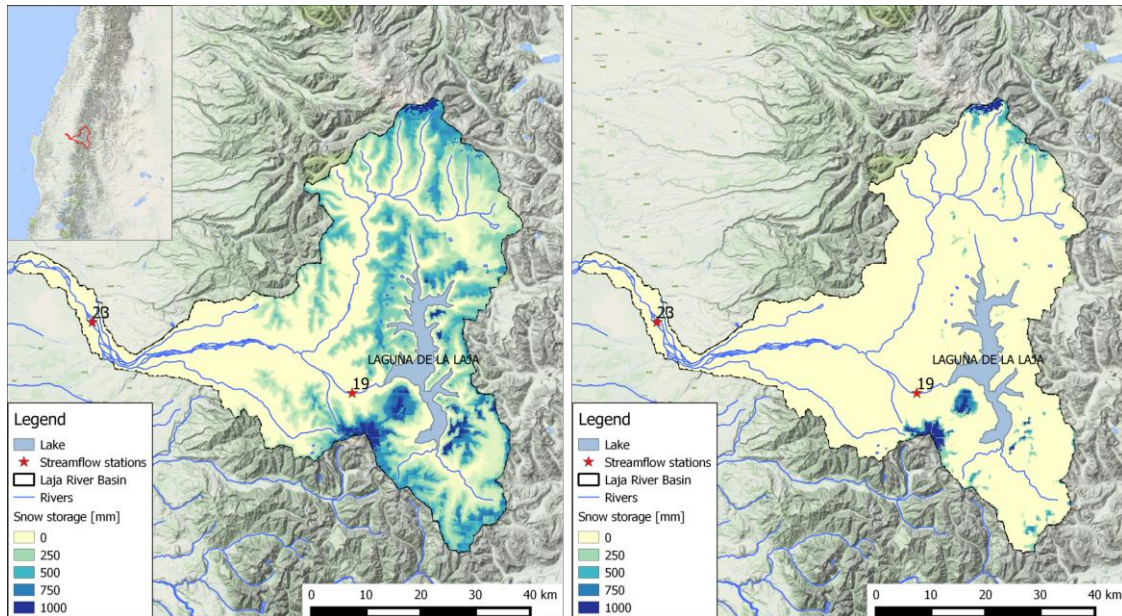


Figure 10: Snow storage (mm) as simulated by the SPHY model on 12 August (left) and 01 October (right) during the snow melting season of 2013 in the Laja River basin.

The hydropower company's main interest is the model's capacity to predict the total expected flow for the coming weeks during the melting season (October 2013 through March 2014). To forecast streamflow during the snow melting season, the SPHY model was forced with gridded temperature and precipitation data from the European Centre for Medium-range Weather Forecasts (ECMWF) Seasonal Forecasting System (SEAS) (Andersson 2013). The SEAS model provided daily forecasts at a spatial resolution of 0.75, 7 months ahead, and was used to forecast streamflow up till the end of the melting season. Figure 12 shows the bias between the total cumulative forecasted flow and observed flow for the 23 model runs that were executed during operational mode. Although there are some bias fluctuations in the Rio Laja en Tucapel model runs, it can be concluded that the bias decreases for each next model run for both locations, which is a logical result of a decreasing climate forcing uncertainty as the model progresses in time. It can be seen that the SPHY model streamflow forecasts for Canal Abanico, which is downstream of Laja Lake, are substantially better than for Rio Laja en Tucapel (the most downstream location). The reason for this has not been investigated during the demonstration study, but since model performance for these two locations was satisfactory during calibration, a plausible explanation could be the larger climate forecast uncertainty in the higher altitude areas (Hijmans et al. 2005; Rollenbeck and Bendix 2011; Vicuña et al., 2011; McPhee et al. 2010; Mendoza et al., 2012; Ragetti and Pellicciotti 2012; Ragetti et al. 2014) in the northeastern part of the basin that contributes to the streamflow of Rio Laja en Tucapel. Additionally, only two in situ meteorological stations were available during operational mode, whereas during calibration, 20+ meteorological stations were available. Moreover, these operational meteorological stations were not installed at higher altitudes, where precipitation patterns tend to be spatially very variable (Wagner et al. 2012; Rollenbeck and Bendix 2011).

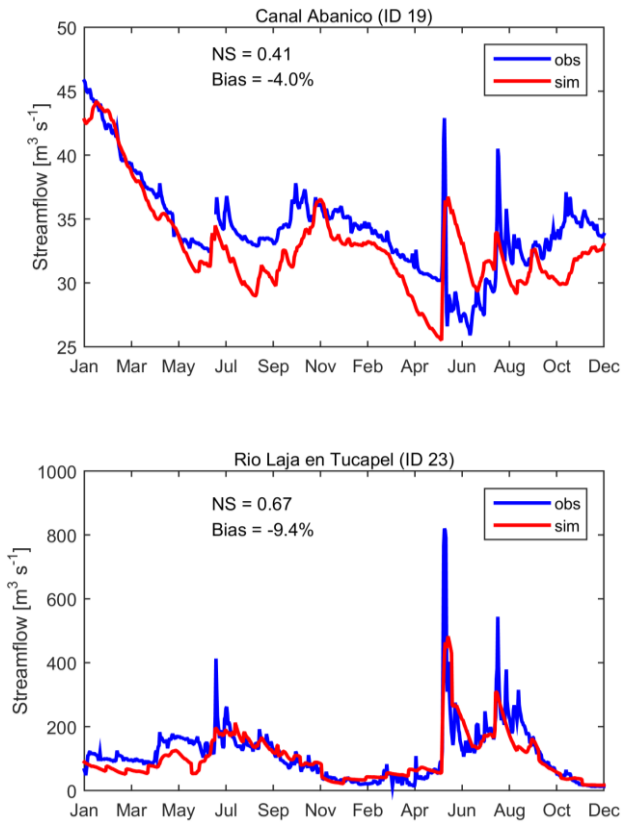


Figure 11: Daily observed vs. SPHY simulated streamflow (period 2007–2008) for the streamflow stations Canal Abanico (ID 19) and Rio Laja en Tucapel (ID 23). The Nash–Sutcliffe (NS) and bias model performance indicators are shown as well.

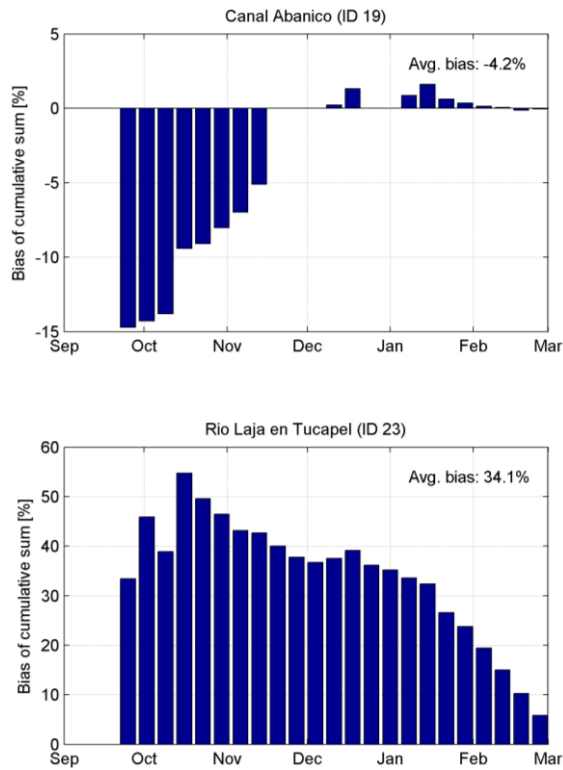


Figure 12: Bias between total cumulative forecasted flow and observed flow for the 23 model runs that were executed between the end of September 2013 and March 2014.



Results are shown for the locations Canal Abanico (ID 19) and Rio Laja en Tucapel (ID 23).



4 Installation of SPHY

4.1 General

SPHY v2.0 can be either be installed as i) a stand-alone application, where the user can run the model throughout the command prompt, or as ii) a an integrated application (plugin) in QGIS, where the model can be run using a Graphical User-Interface (GUI). The GUI has been developed as a plugin in QGIS¹, and has the advantage that changing the model input and output, as well as changing model parameters, is more clear and user-friendly. Furthermore, the use of the plugin allows you to store and visualize your model input and output in the user-friendly and world-wide used QGIS Geographical Information System (GIS), which is in the public domain. The name of this SPHY model plugin is “SphyPlugin” (v1.0), and is compatible with SPHY (v2.0). The installation of the SPHY model plugin is not part of this manual and is described in the SPHY GUIs manual (Terink et al., 2015b).

This manual (Section 4.2) describes the installation of SPHY v2.0 as a stand-alone application.

4.2 Installing SPHY as a stand-alone application

In order to install SPHY as a stand-alone application it is required to have a PC with a windows operating system. The software packages that are required to run the SPHY model as stand-alone application are:

1. Python 2.7.6, 32-bit
2. NumPy 1.8.0, 32-bit
3. PCRaster 4.0, 32-bit
4. SPHY v2.0 source code

These packages need to be installed in the same order as shown above, and the installation of the each package is described in the following sections. The Python, NumPy, and PCRaster software packages can also be downloaded from the SPHY model website as zip-files:

[Download additional software](#)

The login credentials that are required for downloading software and data can be obtained from:

<http://www.sphy.nl/software/download-sphy/>

4.2.1 Python 2.7.6 32-bit

SPHY requires the installation of the Python² programming language. PCRaster has been developed using the 2.7.6 version of Python. Since SPHY has been developed using the 32-bit version of PCRaster 4.0, it is required to install the 32-bit version of Python 2.7.6, which can be downloaded from the internet using the link below:

<https://www.python.org/ftp/python/2.7.6/python-2.7.6.msi>

¹ <http://www.qgis.org/en/site/>

² <https://www.python.org/>



After downloading Python it can be installed by double clicking the downloaded file. During installation it will be asked where to install Python. You can choose any location that you prefer. As an example to be used in this manual, we have installed Python in the folder:

c:\Python27\

A final installation step includes setting the environmental variables. In order to do this, follow the steps below:

1. Go to start, then control panel, and type environment in the top-right search window.
2. Click on "Edit the system environmental variables".
3. Click "Environmental Variables" in the bottom-right of this window (Figure 13).
4. Under system variables, select the Path variable and click "Edit" (Figure 14).
5. In order let your system know the existence of your Python installation, it is required to add your Python installation folder to the "Path" system variable. This is shown in Figure 15 for our case, which was the c:\Python27 installation folder. It is important to have a semicolon between the system variables.
6. Finally, click OK and OK again in order to complete the installation of Python.

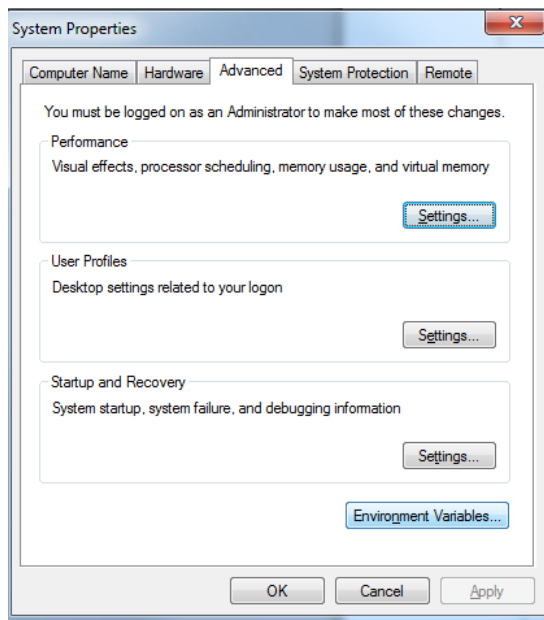


Figure 13: System properties to set Environmental Variables.

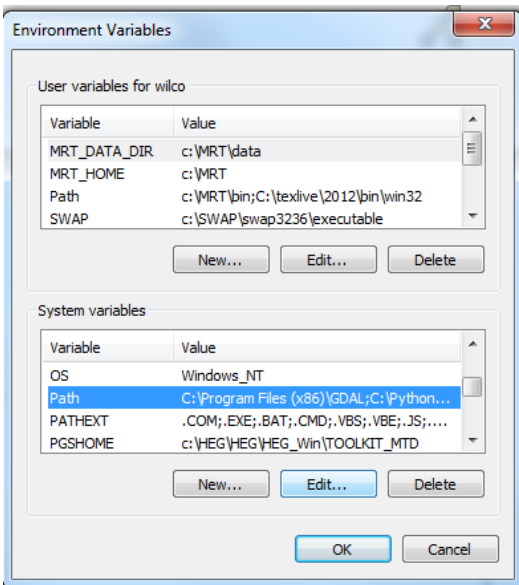


Figure 14: Setting the Path variable.

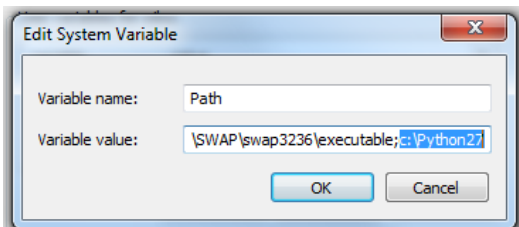


Figure 15: Adding the Python27 installation folder to the Path system variables.

4.2.2 Numpy 1.8.0 32-bit

Numpy stands for Numerical Python, and is a fundamental package for scientific computing with Python. It has especially been developed to work with raster data (arrays), which is also the basis of the PCRaster dynamic modelling framework in which SPHY has been developed.

SPHY requires a Numpy version that works with the 32-bit version of Python 2.7.6, which is Numpy 1.8.0 32-bit. This package can be downloaded using the link below:

<http://sourceforge.net/projects/numpy/files/NumPy/1.8.0/numpy-1.8.0-win32-superpack-python2.7.exe/download>

After downloading the Numpy package, it can be installed by double-clicking on the downloaded file. If Python 2.7.6 has been installed correctly in the previous step, then the Python installation folder will be found automatically during the installation of Numpy. In our example case this folder was c:\Python27\ (see example Figure 16).



numpy-1.8.0

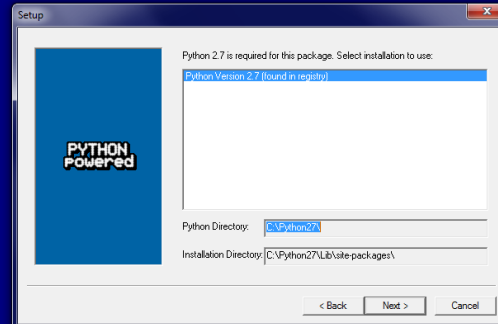


Figure 16: Illustration of selecting the Python installation folder during installation of the Numpy package.

4.2.3 PCRaster 4.0 32-bit

SPHY is written in the Python programming language using the PCRaster (Karsenberg et al., 2001; Karsenberg, 2002; Karsenberg et al., 2010; Schmitz et al., 2009, 2013) dynamic modelling framework. PCRaster¹ has been developed at Utrecht University. PCRaster is targeted to the development and deployment of spatio-temporal environmental models. It allows users to develop their own simulation models for applications in environmental sciences, such as e.g. hydrology, ecology, geography, etc.

SPHY v2.0 is based on the 32-bit system architecture, and therefore requires the 32-bit PCRaster 4 version. SPHY v2.0 has been built and thoroughly tested using PCRaster 4.0.0, and it is therefore recommended to download and install this stable version of PCRaster. More information about this version of PCRaster can be found at the link below:

<http://pcraster.geo.uu.nl/pcraster-4-0-0/>

In order to install PCRaster 4.0.0, it is mandatory to have successfully installed Python 2.7.6 and Numpy 1.8.0 during the previous two steps (Section 0 and 4.2.2). To install PCRaster 4.0.0 you need to perform the following steps:

1. Download the PCRaster version using this link:
http://sourceforge.net/projects/pcraster/files/PCRaster/4.0.0/pcraster-4.0.0_x86-32.zip/download?use_mirror=heanet
2. Create a new folder on your hard disk where you prefer to install PCRaster. For example: c:\Program Files (x86)\PCRaster40\
3. Unzip the contents of the file downloaded under 1) to this folder
4. To let your system recognize the existence of PCRaster, the Environmental Variables need to be updated again. The steps to get to your system Environmental Variables are shown in Section 0, steps 1-4.

¹ <http://pcraster.geo.uu.nl/>



5. It is now required to add the “bin” directory of the extracted PCRaster package to the “Path” system variable (Figure 17). In our example it is the folder: c:\Program Files (x86)\PCRaster40\bin\
6. Click OK.
7. The next step involves setting the PYTHONPATH environment variable. In the same system variables window check the existence of a PYTHONPATH variable. If it exists, then edit the variable by adding the path (Figure 18) of the Python directory of the extracted PCRaster package, which is in our example:

c:\Program Files (x86)\PCRaster40\python\

Otherwise click “New” to create it, and add PYTHONPATH as Variable name, and add the Python directory folder as the Variable value.

8. Click OK and OK to complete the installation of PCRaster.
9. The successful installation of PCRaster can be tested as follows:
 - a. Open a command prompt
 - b. Type *pcrcalc*
 - c. You should see the command prompt view as is shown in Figure 19
10. To test the combination of PCRaster and Python:
 - a. Open a command prompt
 - b. Type *python*
 - c. This opens the Python interactive console
 - d. Type *import pcraster*
 - e. If no errors are shown, then installation has been completed successfully.

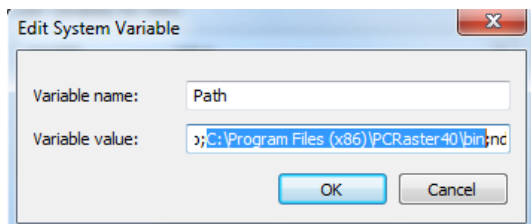


Figure 17: Adding the PCRaster bin folder to the Path system variables.

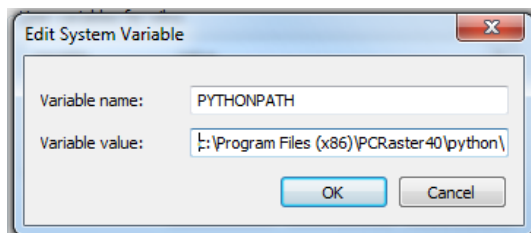


Figure 18: Editing or creating the PYTHONPATH variable for the PCRaster package.



```
Command Prompt
Microsoft Windows [Version 6.1.7601]
Copyright (c) 2009 Microsoft Corporation. All rights reserved.

C:\Users\wilco>pcrcalc
pcrcalc Dec 4 2013 (win32/msvc)
USAGE: pcrcalc [options] "expression"
or pcrcalc [options] -f scriptFile
< or #?: pcrcalc -F [options]+>
other flags:
s # : set seed (integer > 0) for random generator
      default is based on current time
b f : overrule script bindings
l : update timeseries files at end of each timestep
r f : set run directory
d f : debug mode, check MU creation on assignment
      comparing against clone or areamap boolean mask
c : strict Case significant filename check (Unix portability)
p : print profile information
m : optimize with areamap MU compression
l : use less memory but more temporary disk storage
t : test argument substitution

C:\Users\wilco>
```

Figure 19: Command prompt view of testing a successful installation of PCRaster after entering the *pcrcalc* command.

4.2.4 SPHY v2.0 source code

The SPHY v2.0 source code can be obtained from the SPHY model website (<http://www.sphy.nl/software/>). The source code is available as a zip-file (SPHY2.0.zip) and needs to be extracted to a folder on your hard drive. In our case we created the folder c:\SPHY and unzipped the contents of SPHY2.0.zip to this folder. After unzipping the contents of SPHY2.0.zip to a folder of your preference, installation has been completed successfully. The SPHY model v2.0 source code can be downloaded directly using the link below:

[Download SPHY v2.0](#)

The login credentials that are required to download software and data from the SPHY model website can be obtained using the link below:

<http://www.sphy.nl/software/download-sphy/>



5 Build your own SPHY-model

A SPHY model preprocessor has been developed that enables the user to automatically generate SPHY model input data for a selected area of interest. This preprocessor has been developed as a plugin for QGIS, and generates the input data using a database that can be selected by the user. Currently, only one database can be used by the preprocessor: the “Hindu Kush-Himalaya” database. The name of the SPHY model preprocessor is “SphyPreProcess” (v1.0), and is described together with the SPHY model plugin in the SPHY GUIs manual (Terink et al., 2015b).

If your area of interest is not covered by the extent of the database, then you can choose to create your model input data manually (as is done in the Pungwe case-study (Terink et al., 2015a)). You will need the PCRaster command line functions and GIS software, like the open source QGIS. The steps that are required to do this are described in the sections below.

5.1 Select projection extent and resolution

First you need to start a new project within QGIS. Give it a useful name and save your project regularly during the steps in the following sections. Because all calculations in SPHY are metric, you will need to project your data in a metric coordinate system. In the example of the Pungwe basin, we chose the WGS84 UTM Zone 36 South projection (EPSG:32736). Define the minimum and maximum x and y values in the projection that you have chosen that cover the entire area you want to model. Then, define the spatial resolution of your model. The choice of resolution will be a tradeoff of the resolution of your input data, computation resources availability, number of runs you intend to do and required detail for your modelling purpose. For your reference, the model for the Pungwe case study has an extent of 275 x 255 km. For this model the spatial resolution is 1000 x 1000 m, and thus the model contains ~70.000 grid cells. Running this model at a daily time step for 5 years takes about 5 minutes.

In order to create your own model, you need to setup the directory structure. This means you need to create a new **SPHY** model directory (containing the SPHY model source *.py files) and in that directory you need to create a new **input** and **output** directory.

5.2 Clone map

You will need to define a ‘clone’ map, which is a map in PCRaster format, with the model extent and resolution. This map is used as the ‘template’ for your model. You can create a clone map using PCRaster’s [mapattr](#) command in the Windows Command line window. Make sure you are in the model’s **input** directory. This can be done using commands as for example:

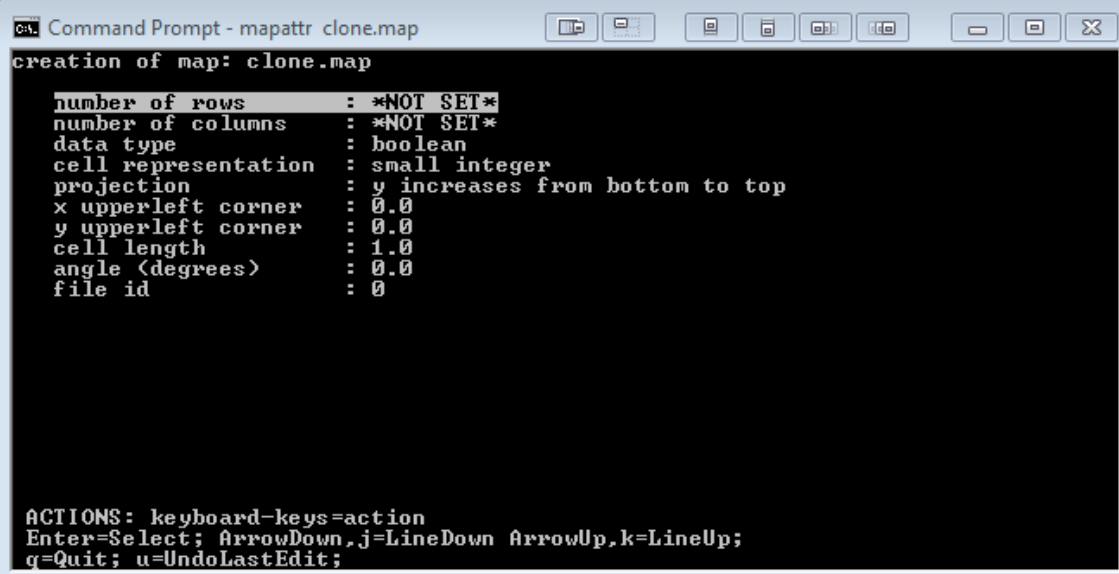
- c: *enter* → go to your c-drive
- cd c:\SPHY\input *enter* → go to the SPHY\input directory on your c-drive
- d: *enter* → go to your d-drive
- cd d:\SPHY\input *enter* → go to the SPHY\input directory on your d-drive
- etc.

If you are in the model’s input directory, then type following in the Command line:

```
mapattr clone.map
```



You will enter a menu, where you can set the clone map's properties:



```
cmd: Command Prompt - mapattr clone.map
creation of map: clone.map

number of rows      : *NOT SET*
number of columns   : *NOT SET*
data type           : boolean
cell representation : small integer
projection           : y increases from bottom to top
x upperleft corner  : 0.0
y upperleft corner  : 0.0
cell length         : 1.0
angle (degrees)     : 0.0
file id             : 0

ACTIONS: keyboard-keys=action
Enter=Select; ArrowDown,j=LineDown ArrowUp,k=LineUp;
q=Quit; u=UndoLastEdit;
```

Figure 20: Command line menu for clone creation

Change the settings of the number of rows, number of columns, check if the y values in your model projection increase from bottom to top or from top to bottom, define the x and y values of the upperleft corner of your model's extent, and define the cell length (spatial resolution).

When all is set, press "q" to quit and then press "y" to confirm the map creation. Then drag the newly created map into QGIS to check if the map has the correct extent. Remember to set the CRS of the "clone.map" after dragging the map into QGIS.

5.3 DEM and Slope

Before you continue with the next steps, make sure that you have opened the "Processing Toolbox" in QGIS (see Figure 21). Next make sure that you select the "Advanced interface" from the "Processing Toolbox" (see Figure 22).

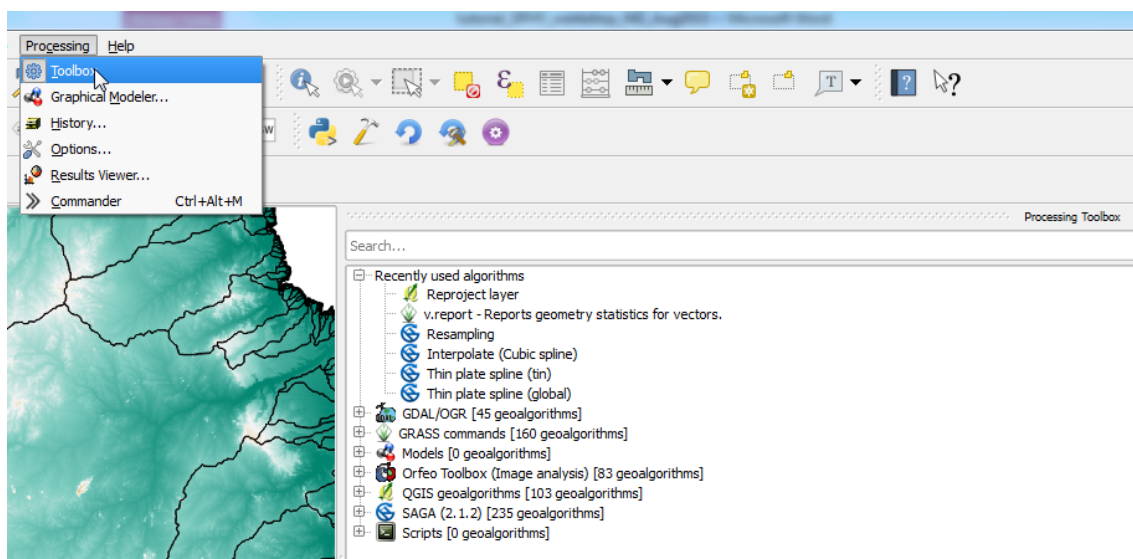


Figure 21: Opening the "Processing Toolbox".



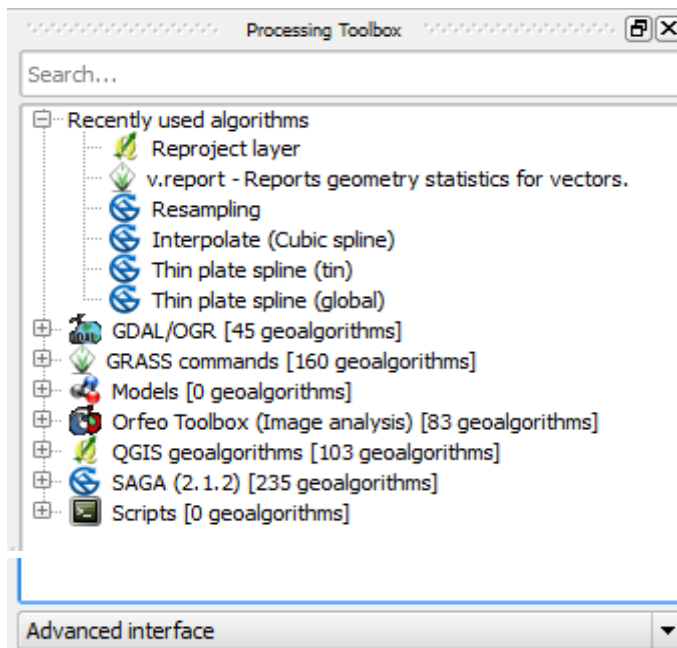


Figure 22: Selecting the “Advanced interface” in the “Processing Toolbox”.

Use your own DEM or otherwise the DEM provided in the database. You will need to project your DEM in the model's projection and resample the DEM to model resolution and extent. You can do that using the following steps:

1. Drag the DEM inside the QGIS canvas;
2. Use the Warp tool in QGIS to reproject the DEM to the Coordinate Reference System (CRS) of your basin (EPSG:XXXXXX). This can be found under Raster → Projections → Warp (Reproject) (see Figure 23).
3. Within the Warp tool you need to select the “*Input file*”, the “*Output file*”, and the “*Target SRS*”. The “*Input file*” is the layer that you need to reproject, which is in this case the **dem**. The “*Output file*” is the file to which you want to save the reprojected **dem** in GeoTiff format (*.tif). Give it a useful name and save it in a directory that is useful. In the example of Figure 24, the reprojected dem is saved under the **SPHY/input/** directory with the name: **dem_pr.tif**. Finally, it is important that you select the correct “*Target SRS*” (EPSG:XXXXX), which you defined in Section 5.1. In the example of Figure 24 it is EPSG:32737. Then click OK to do the reprojection. After the reprojection is finished click OK, and again OK, and finally Close.



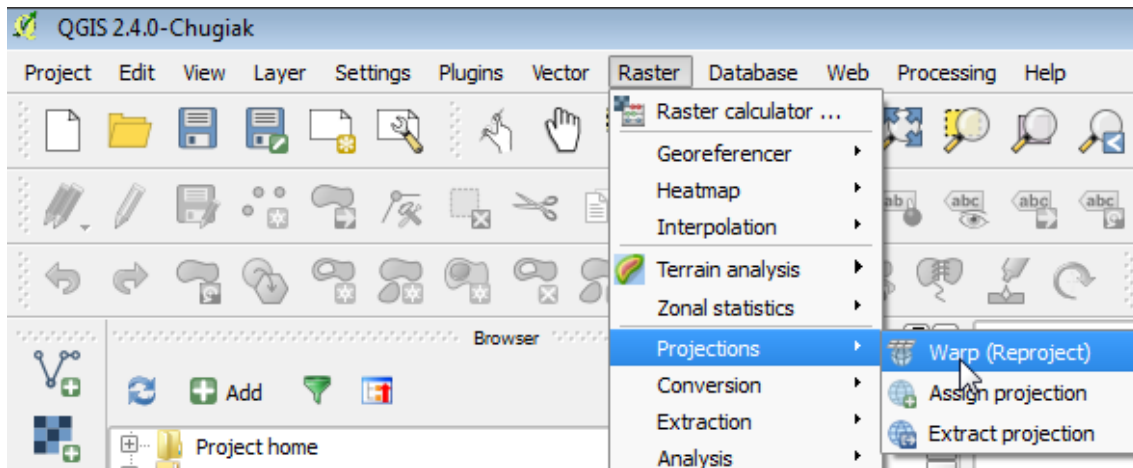


Figure 23: Warp tool

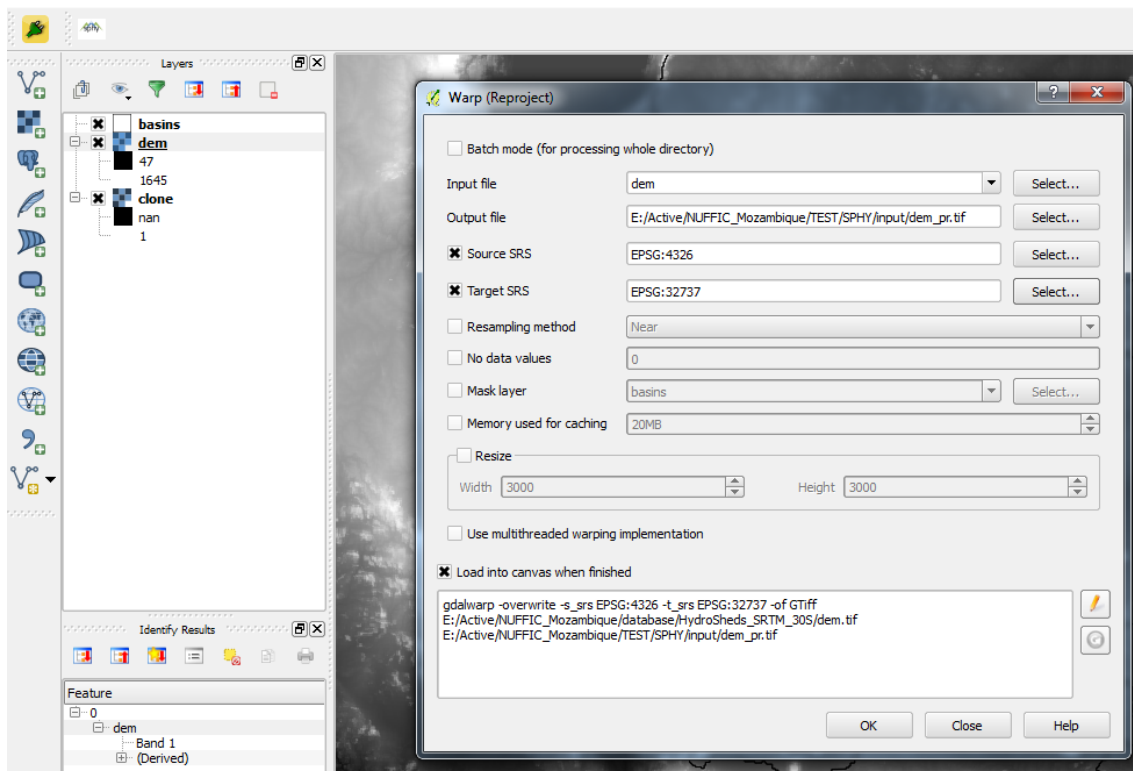


Figure 24: Setting the files and Source and Target SRS in the Warp Tool.

4. The next step involves resampling the projected dem from step 3) to the extent and spatial resolution of the **clone.map**. For this you need to type "resampling" in the "Processing Toolbox" search window (see Figure 25).



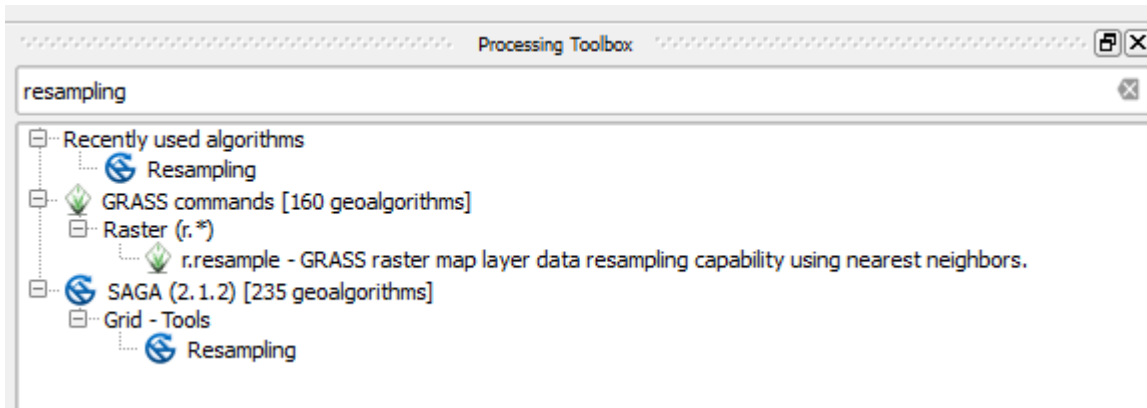


Figure 25: Selecting the Resampling tool in the Processing Toolbox.

5. Then double click “Resampling” under SAGA → Grid – Tools to open the *Resampling* tool as shown in Figure 26.
6. Within this tool you need to select the “Grid” file that you want to resample, the “Interpolation Methods” for scaling up and for scaling down, the “Output extent”, the “Cellsize”, and the “Grid” to which you want to save the resampled file. You also need to check or uncheck the “Preserve Data Type” option. You can use Table 4 to determine which options to set for the “Preserve Data Type”, and the “Interpolation Methods” for scaling up and for scaling down.

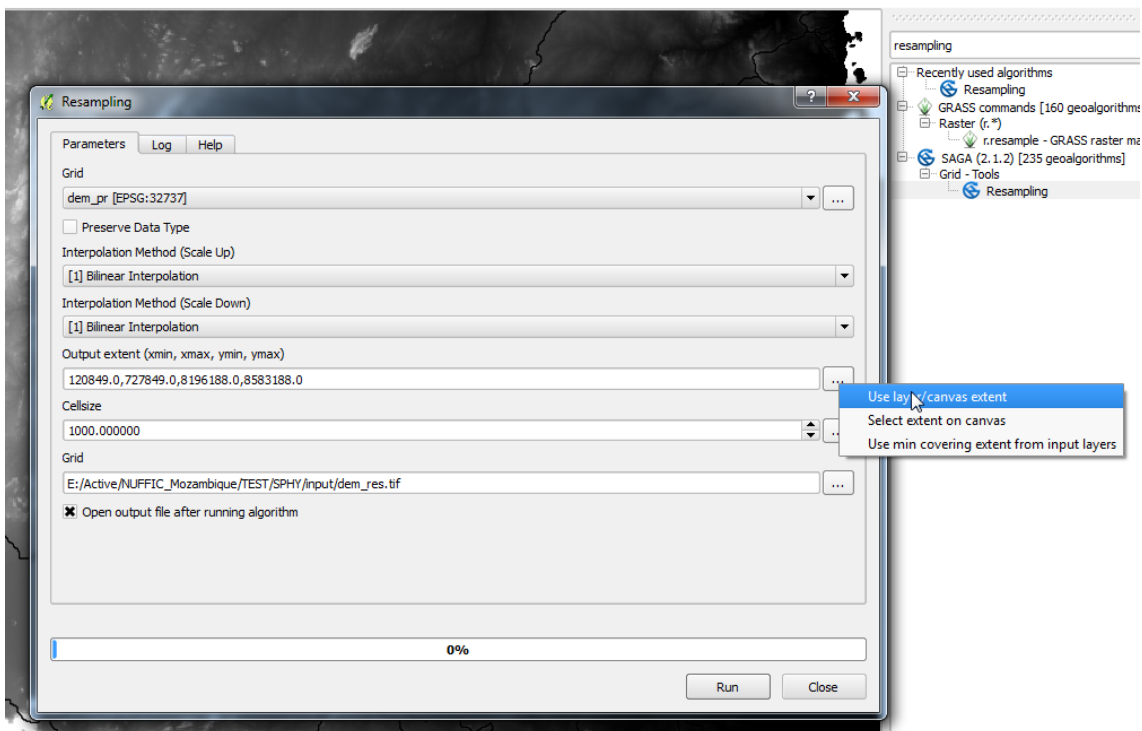


Figure 26: Setting the Resampling tool options.



Table 4: Resampling settings based on the layer data type.

Layer data type	Preserve Data Type	Data	Interpolation Method (scale Up)	Interpolation Method (scale Down)	Example layer
Continuous	No		Bilinear	Bilinear	DEM
Classified	No		Majority	Nearest neighbor	Landuse

- Since the projected dem that we want to resample is continuous data, we select “*Bilinear Interpolation*” for both the interpolation methods, and we uncheck the “*Preserve Data Type*” option. For the “*Grid*” we select the projected dem from step 3). For the “*Output extent*” we use the layer extent (see Figure 26) of the **clone.map**. For the “*Cellsize*” (=cell length) you can fill in the value that you determined in Section 5.1. Then, save the resampled Grid as GeoTiff in the “*Grid*” in a useful directory. In the example of Figure 26 the file is saved as **dem_res.tif** under the directory **SPHY/input/**. Finally, click Run to finish the resampling. If these steps are performed correctly, then your resampled **dem** should have the same extent and spatial resolution as your **clone.map**.
- The final step involves converting the GeoTiff format to the PCRaster *.map format. This can be done using the Translate function under Raster → Conversion → Translate (Convert Format) (see Figure 27).

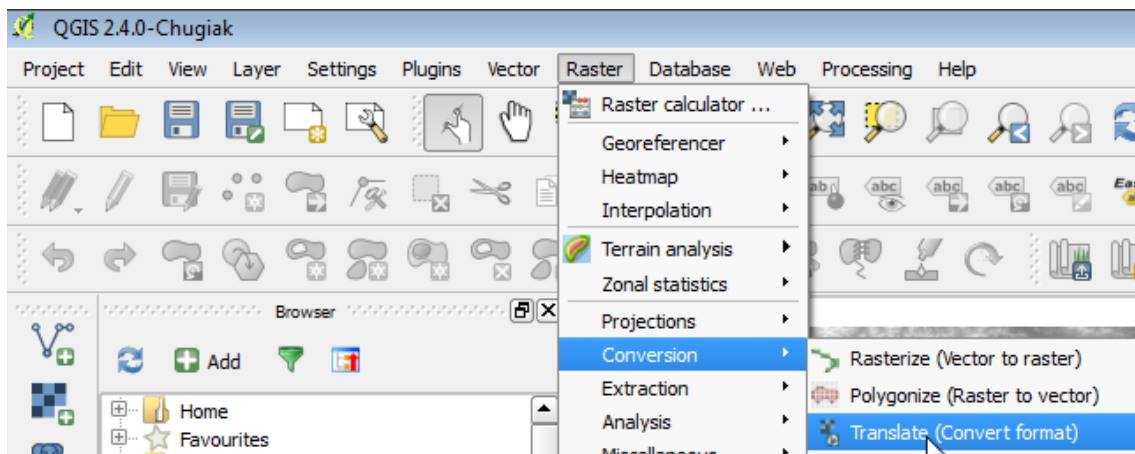


Figure 27: Translate tool (convert raster format)

- In the “*Translate*” box (see Figure 28) make sure that you select the “*Input Layer*” (result from step 7) and set the “*Output Layer*”. The “*Output Layer*” should be save as PCRaster Raster File format (*.map). In the example of Figure 29 we save it in the **SPHY\input** directory with the name **dem.map**. Finally click OK, and OK, and OK, and Close to finish this step.

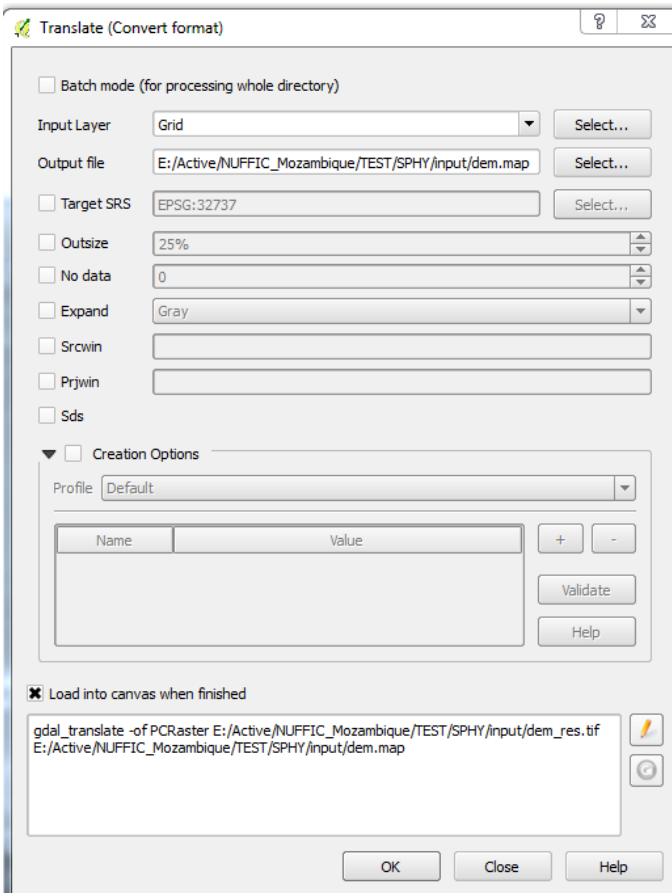


Figure 28: Setting the Translate options.

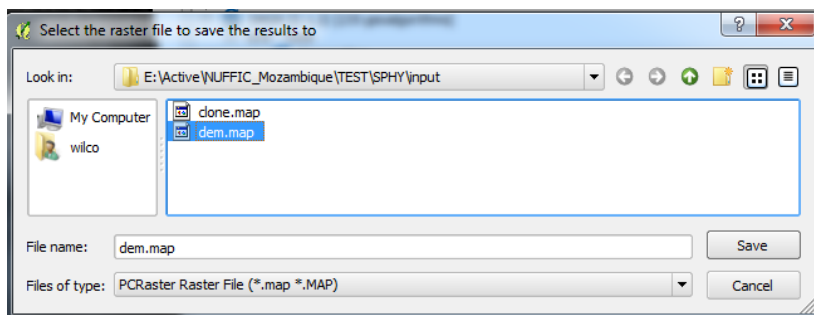


Figure 29: Saving the translated raster as a PCRaster Raster File (*.map).

Now you should have the DEM in the model resolution and extent and in PCRaster format.

The slope map can be derived from the DEM using the [slope](#) command. This can be done in the Windows Command line window by typing:

```
pcrcalc slope.map = slope(dem.map)
```

5.4 Delineate catchment and create local drain direction map

You can now use the DEM you created in the previous section to generate a local drain direction (LDD) map for your own model area.



To create a flow direction map (or local drain direction (LDD)), you can use the pcraster command `lddcreate`. Type the following command in the Windows Command line window:

```
pcrcalc ldd.map = lddcreate(dem.map, 1e31,1e31,1e31,1e31)
```

This command should also fill the sinks in the DEM to avoid that pits are generated in the depression in the DEM, which could hamper the water to flow to the basin's outlet. A good way to test if the LDD map is correct is to calculate for each cell how many cells are upstream. You can do this using the pcraster command `accuflux`. Type:

```
pcrcalc accuflux.map = accuflux(ldd.map, 1)
```

Drag the newly generated `accuflux.map` to the QGIS canvas. Check if the stream network is complete, and all branches are connected to the outlet point.

If the generated LDD is not entirely correct and not all streams are connected toward the downstream outlet point, this happens because during the creation of the LDD map, pits have been generated where depressions in the landscape are present. More details on the LDD generation can be found in the PCRASTER online manual. There are multiple ways to overcome the problem of pit generation. The first and most easy option is to try this command in the Windows Command line window:

```
pcrcalc ldd.map = lddrepair(ldd.map)
```

If this does not solve the correct creation of the `ldd.map`, then you can try the following options:

- Test different values for the parameters in the `lddcreate` command
- Remove pits manually by changing the values for those cells.
- Use a map with the streams present in your study area and “burn” them into the DEM to force the other cells to drain in into them.

5.5 Preparing stations map and sub-basins.map

To prepare a stations map it is easiest to use a vector file with the point locations (for example a shapefile), to a PCRaster grid (.map file). You can create a new shapefile with points in QGIS under Layer → New → New Shapefile layer:

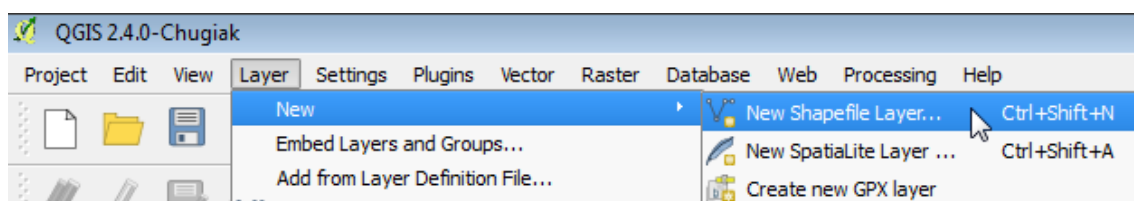


Figure 30: Create new shapefile layer

Make sure that you select “Point” and that the CRS corresponds (see Figure 31) with the EPSG that you have defined in Section 5.1. Finally click OK to create the New Shapefile Layer and save it under a useful name, for example **locations.shp**.



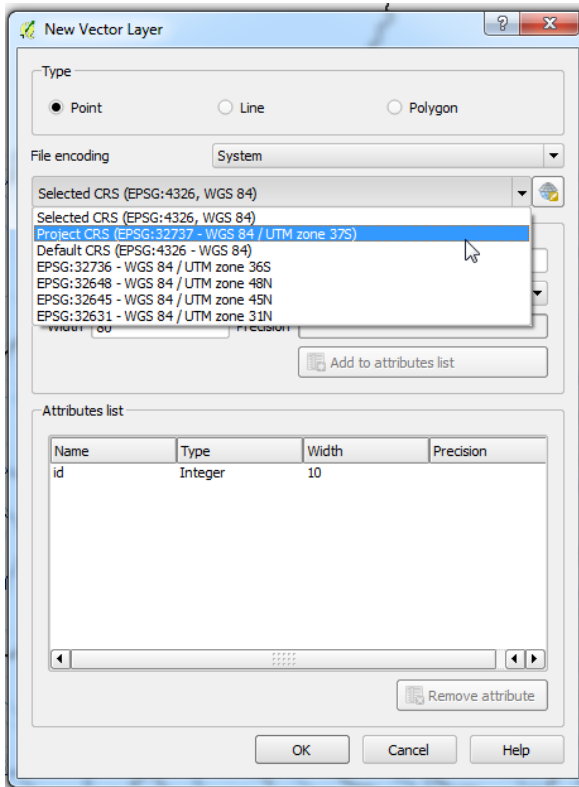


Figure 31: Setting the properties of the New Shapefile Layer.

The next step involves adding points to the Shapefile where you want the SPHY model to report time-series. Often these points correspond with the locations of discharge measurement stations. If you have an existing Shapefile of discharge measurement stations in your basin, then you can easily drag this file into QGIS to identify these locations. Now you can start adding points to the newly created Shapefile by following these steps:

1. Make sure the “*locations*” layer is selected. Then click “*Toggle Editing*” to change the layer to editing mode (see Figure 32).

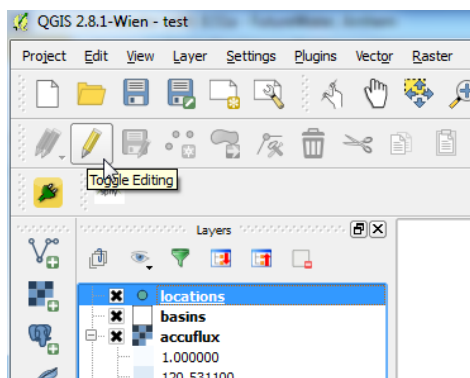


Figure 32: Toggle Editing for Shapefiles.

2. Then click the “*Add Feature*” option (see Figure 33). Now you can start adding points to the map where you want the SPHY model to create time-series output. The **accuflux.map** can help you determining if you are adding a point to the river network. Add as many as points as you like. For each point you need to provide an ID number. Start with ID 1, then ID 2, etc. In the example of Figure 34 we added 3 points to the “*locations*” layer.



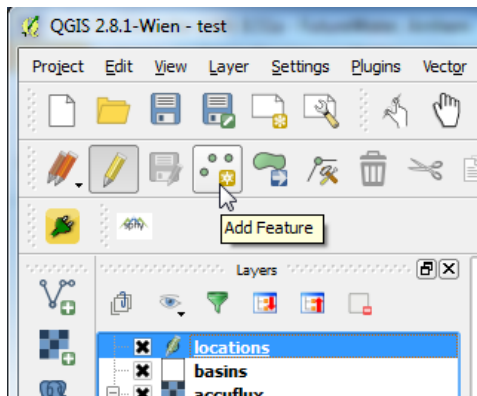


Figure 33: Add Feature for Shapefiles.

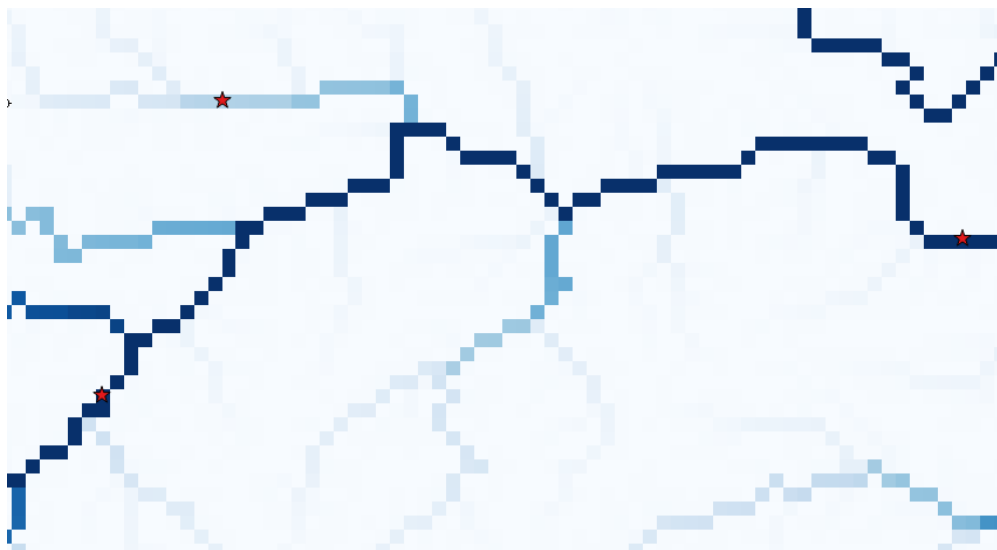


Figure 34: Adding points to the locations Shapefile layer using the accuflux.map.

3. If you are finished with adding the points, then you again can click the *“Toggle Editing”* button and Save your edits.
4. The next step involves converting the *“locations”* Shapefile layer to a raster layer. This can be done using the *“v.to.rast.attribute”* tool in QGIS under Processing Toolbox (see Figure 35).
5. Within this toolbox (Figure 36) set the *“locations”* layer as *“Input vector layer”*, make sure that the *“id”* column is selected, set the *“GRASS region extent”* by specifying the **clone.map** layer, and set the *“GRASS region cellsize”* as determined before. Finally, choose a *“Rasterized”* layer name (e.g. *“locations.tif”*) and click Run.
6. The final step again involves converting the resulting GeoTiff raster from step 5) to a PCRaster *.map format. This can be done using the Raster → Conversion → Translate tool (see Figure 27 and Figure 28). The only additional step required here is to click the *“Edit”* button (see Figure 37) and add the following syntax: **-ot Float32** (see Figure 38).
7. Finally click OK, and again OK, and again OK, and Close to finish the conversion.



Figure 35: Selecting the v.to.rast.attribute tool from the Processing Toolbox.

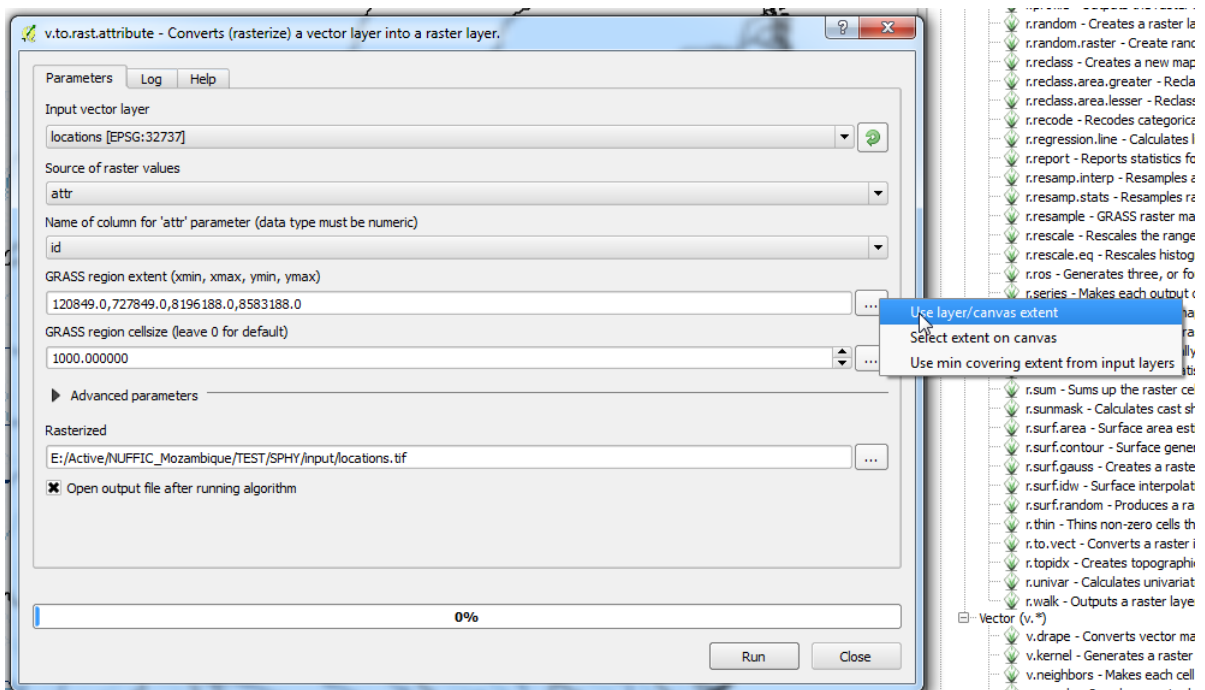


Figure 36: Setting the options in the v.to.rast.attribute tool.



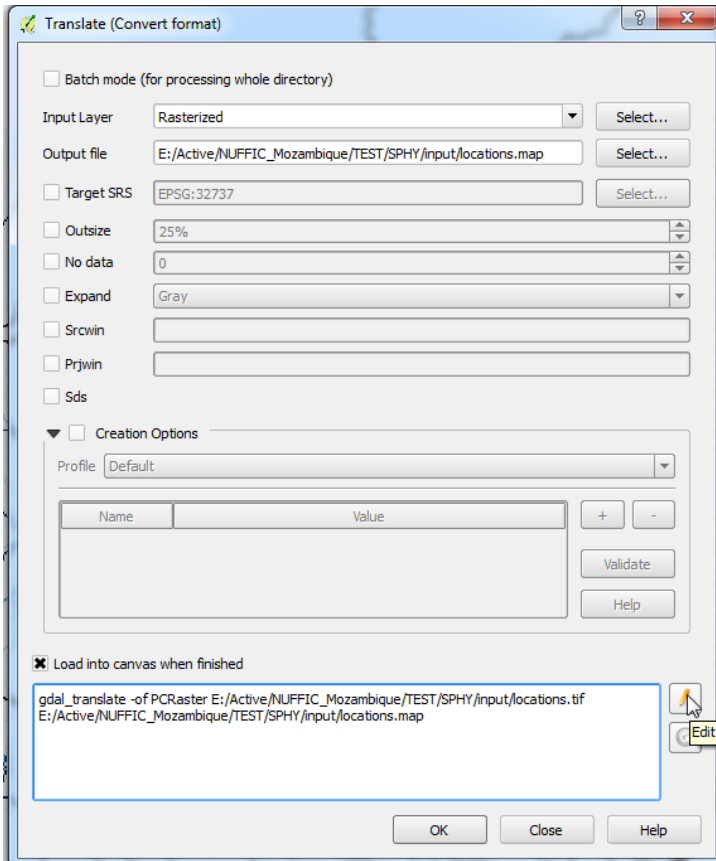


Figure 37: Editing the command for Translation.

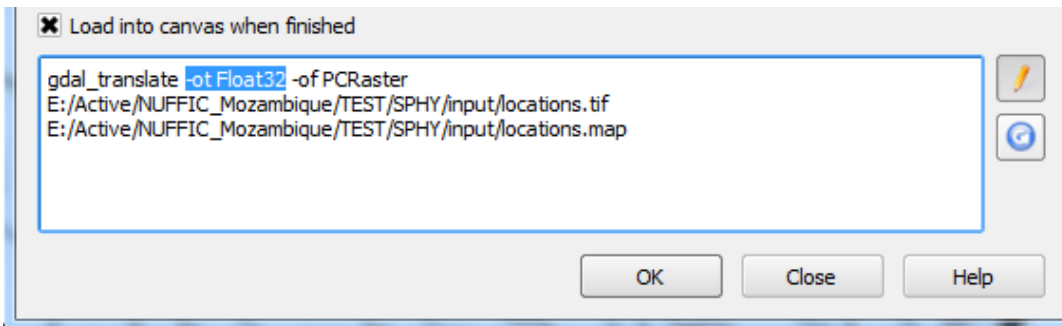


Figure 38: Adding the “-ot Float32” syntax to the command for Translation.

The resulting “*locations.map*” is of the Float32 data format (scalar). As can be seen Table 5 from it is required to have a nominal format for station files. This can be achieved by typing the following command in the Windows Command line:

```
pcrcalc locs.map = nominal(locations.map)
```

You can use **locs.map** and **ldd.map** to delineate the catchments of the points in **locs.map**. Use the [subcatchment](#) command for that:

```
pcrcalc catchment.map = subcatchment(ldd.map, locs.map)
```



5.6 Glacier fraction map

The glacier fraction map can be calculated from a vector file with glacier outlines. In QGIS from the Processing toolbox, select the “*v.to.rast.value*” tool like in the previous section.

Select your glacier outlines as vector input layer and convert it to raster at the same extent of the clone map. Set the cellsize at a lower value than your model resolution. For example, if your model cell size is 200 m, select 20 m for the converted raster.

The “*nodata*” values need to be reclassified to zeros. To do this use SAGA’s Reclassify tool from the Processing toolbox. You can easily find it by typing Reclassify in the search field.

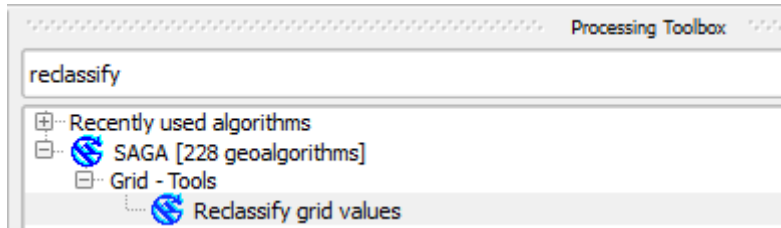


Figure 39: Reclassify tool

In the dialog box set all values to 0.0, and set “*replace no data values*” to “*Yes*”, set “*new value for no data values*” to 0.0 and set “*replace other values*” to “*No*”. Select an output filename and click “*Run*”.



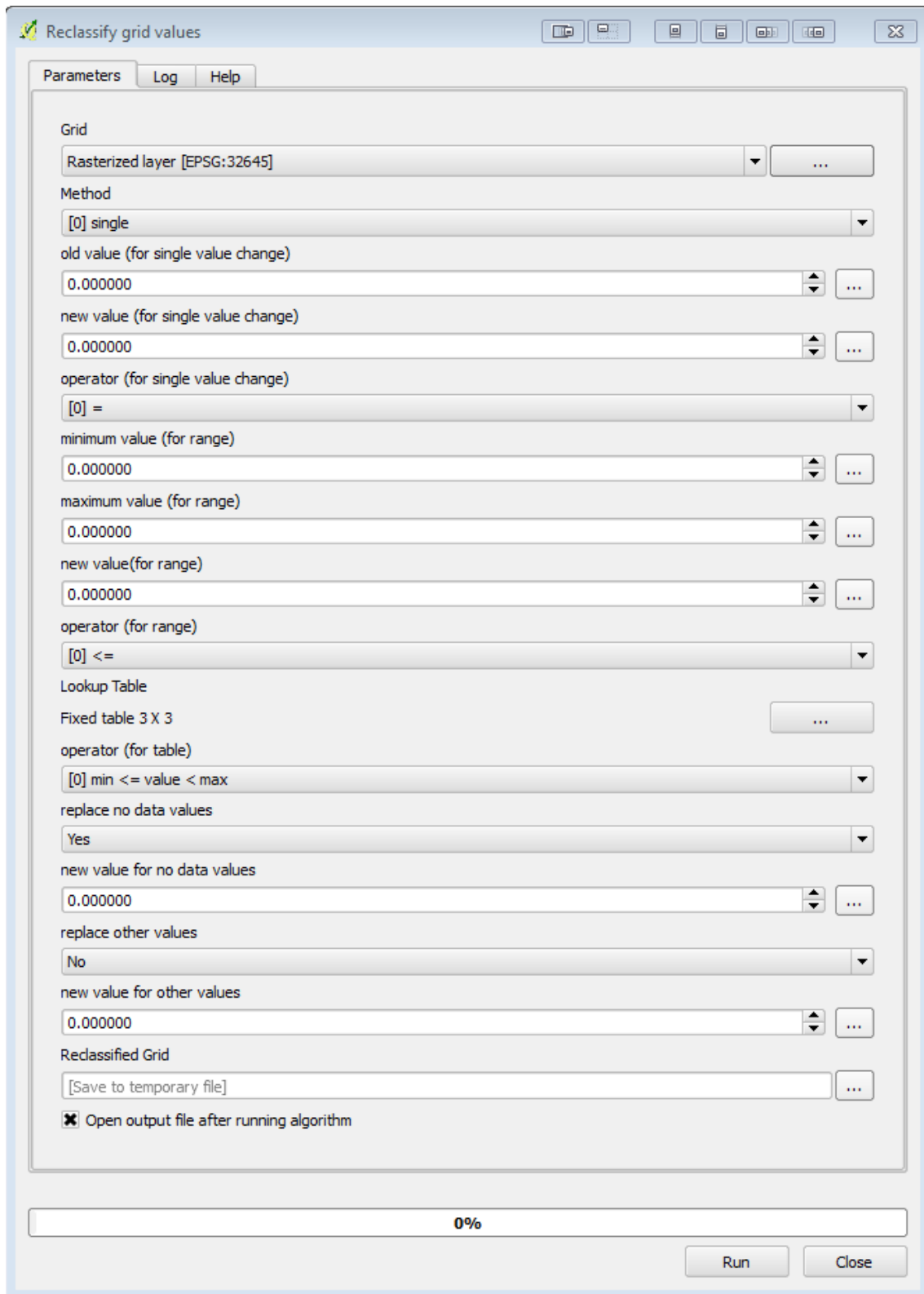


Figure 40: Reclassify tool dialog box

Now we aggregate the fine resolution grid with glaciers to the model resolution. This can be done using the “*r.resamp.stats*” tool selected under Processing Toolbox → GRASS commands → Raster → *r.resamp.stats*.



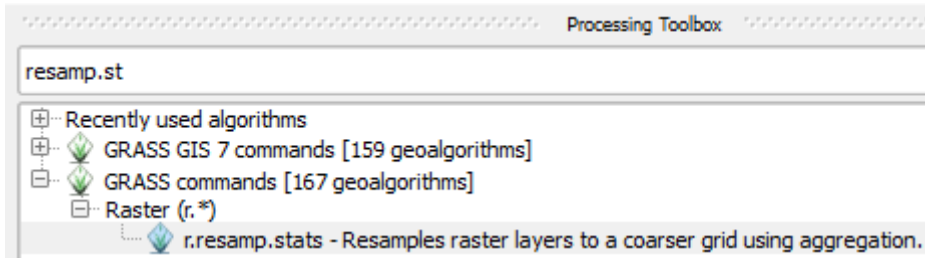


Figure 41: GRASS aggregation tool

In the dialog box, set the fine resolution glacier grid as input raster layer and choose aggregation method “*average*”. Import the processing extent from the clone map and set the cell size to the model resolution (in the screenshot below it is 200m as in the example of the Trisuli case study).

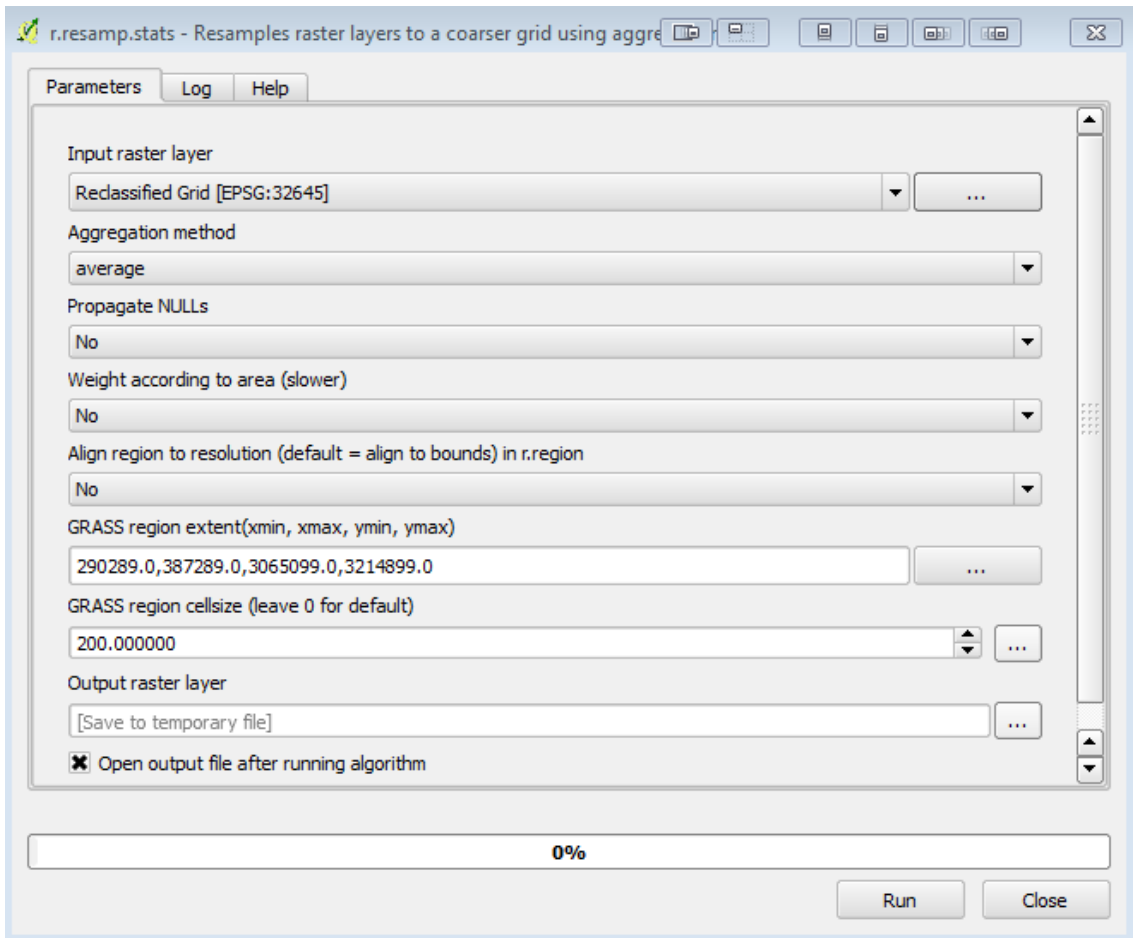


Figure 42: GRASS aggregation tool dialog box

The resulting grid can be converted to a PCRaster map using step 8 from Section 5.3.

5.7 Other static input maps

Similar as the DEM, you can reproject and resample other static model input data and convert them to PCRaster format maps using the reprojection and resampling functions in QGIS (step 1-9 from Section 5.3). Note that different data types are used for PCRaster maps. You can convert maps from one data type to another using the command line functions `boolean()`,



nominal(), ordinal(), scalar(), directional() or ldd(). For example to convert the scalar type landuse.map to a nominal landuse.map, type:

```
pcrcalc landuse_nominal.map = nominal(landuse.map)
```

Table 5: Data types used in SPHY.

data type	description attributes		domain	Example
boolean	boolean		0 (false), 1 (true)	suitable/unsuitable, visible/non visible
nominal	classified, order	no	$-2^{31} \dots 2^{31}$, whole values	soil classes, land use classes, discharge stations, administrative regions
ordinal	classified, order		$-2^{31} \dots 2^{31}$, whole values	succession stages, income groups
scalar	continuous, linear		$-10^{37} \dots 10^{37}$, real values	elevation, temperature
directional	continuous, directional		0 to 2 pi (radians), or to 360 (degrees), and -1 (no direction), real values	aspect
ldd	local direction neighbour cell	drain to	1...9 (codes of drain directions)	drainage networks, wind directions

5.8 Meteorological forcing map series

Meteorological forcing map-series are series of input maps with the time step indicated in each filename. The filenames have a strict format with 8 characters before a dot (.), and three characters behind the dot. For example the average temperature maps can have the format **tavg0000.001**, **tavg0000.002**, etc. To generate forcing data you have two options:

- 1) interpolate point station data to grids at the model extent and resolution, and convert to PCRaster grid format.
- 2) resample existing gridded meteorological data products to model extent and resolution and convert to PCRaster grid format.

Depending on the number of time steps in your model you will probably need to write a script to batch this process and repeat it automatically for multiple time steps. A script like this can be created in any scripting language like for example Python or R. This procedure is automated in the SPHY preprocessor plugin (Terink et al., 2015b).



6 References

- Abbott, M., Bathurst, J., Cunge, J., O'Connell, P., and Rasmussen, J.: An introduction to the European Hydrological System – Systeme Hydrologique Europeen, "SHE", 2: Structure of a physically-based, distributed modelling system, *J. Hydrol.*, 87, 61–77, 1986.
- ADB: Consultant's Report Regional Technical Assistance: Water and Adaptation Interventions in Central and West Asia, Tech. rep., 2012.
- Allen, R. G., Pereira, L. S., Raes, D., and Smith, M.: Crop evapotranspiration – Guidelines for computing crop water requirements, *FAO Irrigation and drainage paper*, 56, 1998.
- Andersson, E.: User guide to ECMWF forecast products. Version 1.1, Tech. rep., ECMWF, available at: http://old.ecmwf.int/products/forecasts/guide/user_guide.pdf (last access: 02 August 2014), 2013.
- Bartholomeus, R. P., Witte, J.-P. M., van Bodegom, P. M., van Dam, J. C., and Aerts, R.: Critical soil conditions for oxygen stress to plant roots: Substituting the Feddes function by a process-based model, *J. Hydrol.*, 360, 147–165, doi:10.1016/j.jhydrol.2008.07.029, 2008.
- Bastiaanssen, W., Allen, R., Droogers, P., Da'Urso, G., and Steduto, P.: Twenty-five years modeling irrigated and drained soils: State of the art, *Agr. Water Manag.*, 92, 111–125, doi:10.1016/j.agwat.2007.05.013, 2007.
- Batjes, N., Dijkshoorn, K., van Engelen, V., Fischer, G., Jones, A., Montanarella, L., Petri, M., Prieler, S., Teixeira, E., Wiberg, D., and Shi, X.: Harmonized World Soil Database (version 1.1), Tech. rep., FAO and IIASA, Rome, Italy and Laxenburg, Austria, 2009.
- Batjes, N., Dijkshoorn, K., van Engelen, V., Fischer, G., Jones, A., Montanarella, L., Petri, M., Prieler, S., Teixeira, E., Wiberg, D., and Shi, X.: Harmonized World Soil Database (version 1.2), Tech. rep., FAO and IIASA, Rome, Italy and Laxenburg, Austria, 2012.
- Beven, K.: Kinematic subsurface stormflow, *Water Resour. Res.*, 17, 1419–1424, doi:10.1029/WR017i005p01419, 1981.
- Beven, K.: Robert E. Horton's perceptual model of infiltration processes, *Hydrol. Process.*, 18, 3447–3460, doi:10.1002/hyp.5740, 2004.
- Beven, K. and Germann, P.: Macropores and water flow in soils, *Water Resour. Res.*, 18, 1311–1325, doi:10.1029/WR018i005p01311, 1982.
- Bierkens, M. F. P. and van Beek, L. P. H.: Seasonal Predictability of European Discharge: NAO and Hydrological Response Time, *J. Hydrometeorol.*, 10, 953–968, doi:10.1175/2009JHM1034.1, 2009.
- Biswas, A. K. and Tortajada, C.: Future Water Governance: Problems and Perspectives, *Int. J. Water Resour. D.*, 26, 129–139, doi:10.1080/07900627.2010.488853, 2010.
- Bontemps, S., Defourny, P., van Bogaert, E., Arino, O., Kalogirou, V., and Ramos Perez, J.: GLOBCOVER 2009. Products Description and Validation Report, Tech. rep., ESA, 2011.
- Bowling, L. C., Pomeroy, J. W., and Lettenmaier, D. P.: Parameterization of Blowing-Snow Sublimation in a Macroscale Hydrology Model, *J. Hydrometeorol.*, 5, 745–762, doi:10.1175/1525-7541(2004)005<0745:POBSIA>2.0.CO;2, 2004.
- Bracken, C., Rajagopalan, B., and Prairie, J.: A multisite seasonal ensemble streamflow forecasting technique, *Water Resour. Res.*, 46, doi:10.1029/2009WR007965, 2010.
- Bramer, L. M., Hornbuckle, B. K., and Caragea, P. C.: How Many Measurements of Soil Moisture within the Footprint of a Ground-Based Microwave Radiometer Are Required to Account for Meter-Scale Spatial Variability?, *Vadose Zone J.*, 12, 3, doi:10.2136/vzj2012.0100, 2013.
- Brutsaert, W.: De Saint-Venant Equations Experimentally Verified, *J. Hydr. Eng. Div.-ASCE*, 97, 1387–1401, 1971.



- Brutsaert, W.: *Hydrology. An introduction.*, Cambridge University Press, Cambridge, 2005.
- Carlson, T. N. and Ripley, D. A.: On the relation between NDVI, fractional vegetation cover, and leaf area index, *Remote Sens. Environ.*, 62, 241–252, doi:10.1016/S0034-4257(97)00104-1, 1997.
- Clark, M. P., Slater, A. G., Rupp, D. E., Woods, R. A., Vrugt, J. A., Gupta, H. V., Wagener, T., and Hay, L. E.: Framework for Understanding Structural Errors (FUSE): A modular framework to diagnose differences between hydrological models, *Water Resour. Res.*, 44, W00B02, doi:10.1029/2007WR006735, 2008.
- Clark, M. P., Nijssen, B., Lundquist, J. D., Kavetski, D., Rupp, D. E., Woods, R. A., Freer, J. E., Gutmann, E. D., Wood, A. W., Brekke, L. D., Arnold, J. R., Gochis, D. J., and Rasmussen, R. M.: A unified approach for process-based hydrologic modeling: 1. Modeling concept, *Water Resour. Res.*, 51, 2498–2514, doi:10.1002/2015WR017198, 2015a.
- Clark, M. P., Nijssen, B., Lundquist, J. D., Kavetski, D., Rupp, D. E., Woods, R. A., Freer, J. E., Gutmann, E. D., Wood, A. W., Gochis, D. J., Rasmussen, R. M., Tarboton, D. G., Mahat, V., Flerchinger, G. N., and Marks, D. G.: A unified approach for process-based hydrologic modeling: 2. Model implementation and case studies, *Water Resour. Res.*, 51, 2515–2542, doi:10.1002/2015WR017200, 2015b.
- Contreras, S., Hunink, J., and Baille, A.: Building a Watershed Information System for the Campo de Cartagena basin (Spain) integrating hydrological modeling and remote sensing. *FutureWater Report 125.*, Tech. rep., FutureWater, 2014.
- Corradini, C., Morbidelli, R., and Melone, F.: On the interaction between infiltration and Hortonian runoff, *J. Hydrol.*, 204, 52–67, doi:10.1016/S0022-1694(97)00100-5, 1998.
- Dai, A.: Drought under global warming: a review, *Wiley Interdisciplinary Reviews: Climate Change*, 2, 45–65, doi:10.1002/wcc.81, 2011.
- de Jong, S. and Jetten, V.: Distributed, quantitative assessment of canopy storage capacity by Hyperspectral Remote Sensing, available at: <http://www.geo.uu.nl/dejong/pdf-files/Interception-by-RS.pdf> (last access: 13 November 2014), 2010.
- Deb, S. and Shukla, M.: *Soil hydrology, land use and agriculture: measurement and modelling*, Las Cruces, doi:10.1079/9781845937973.0000, 2011.
- Droogers, P. and Aerts, J.: Adaptation strategies to climate change and climate variability: A comparative study between seven contrasting river basins, *Phys. Chem. Earth Pt. A/B/C*, 30, 339–346, doi:10.1016/j.pce.2005.06.015, 2005.
- Droogers, P. and Bouma, J.: Simulation modelling for water governance in basins, *Int. J. Water Resour. D.*, 30, 475–494, doi:10.1080/07900627.2014.903771, 2014.
- Droogers, P. and Immerzeel, W. W.: Wat is het beste model?, *H2O Tijdschrift voor watervoorziening en waterbeheer*, 4, 38–41, 2010.
- Droogers, P., Immerzeel, W. W., Terink, W., Hoogeveen, J., Bierkens, M. F. P., van Beek, L. P. H., and Debele, B.: Water resources trends in Middle East and North Africa towards 2050, *Hydrol. Earth Syst. Sci.*, 16, 3101–3114, doi:10.5194/hess-16-3101-2012, 2012.
- EEA: EU-DEM layers, Copernicus data and information funded by the European Union, European Environmental Agency, Tech. rep., 2014.
- Endrizzi, S., Dall'Amico, M., Gruber, S., and Rigon, R.: *GEOtop Users Manual. User Manual Version 1.0*, Tech. rep., Department of Physical Geography, University of Zurich, Zurich, 2011.
- Endrizzi, S., Gruber, S., Dall'Amico, M., and Rigon, R.: GEOtop 2.0: simulating the combined energy and water balance at and below the land surface accounting for soil freezing, snow cover and terrain effects, *Geosci. Model Dev.*, 7, 2831–2857, doi:10.5194/gmd-7-2831-2014, 2014.



- EPA: Modeling at EPA, available at: <http://www.epa.gov/epahome/models.htm> (last access: 30 September 2014), 2014.
- Essery, R., Morin, S., Lejeune, Y., and B Ménard, C.: A comparison of 1701 snow models using observations from an alpine site, *Adv. Water Resour.*, 55, 131–148, doi:10.1016/j.advwatres.2012.07.013, 2013.
- FAO: FAOWater. CropWater Information, available at: <http://www.fao.org/nr/water/cropinfo.html> (last access: 09 June 2014), 2013.
- Feddes, R., Kowalik, P., and Zaradny, H.: Simulation of field water use and crop yield. Simulation Monographs, Pudoc, Wageningen University, 1978.
- Finger, D., Pellicciotti, F., Konz, M., Rimkus, S., and Burlando, P.: The value of glacier mass balance, satellite snow cover images, and hourly discharge for improving the performance of a physically based distributed hydrological model, *Water Resour. Res.*, 47, W07519, doi:10.1029/2010WR009824, 2011.
- Foglia, L., Hill, M. C., Mehl, S. W., and Burlando, P.: Sensitivity analysis, calibration, and testing of a distributed hydrological model using error-based weighting and one objective function, *Water Resour. Res.*, 45, W06427, doi:10.1029/2008WR007255, 2009.
- Gat, J. R., Bowser, C. J., and Kendall, C.: The contribution of evaporation from the Great Lakes to the continental atmosphere: estimate based on stable isotope data, *Geophys. Res. Lett.*, 21, 557–560, doi:10.1029/94GL00069, 1994.
- Gill, M. A.: Flood routing by the Muskingum method, *J. Hydrol.*, 36, 353–363, doi:10.1016/0022-1694(78)90153-1, 1978.
- Gopalan, K., Wang, N.-Y., Ferraro, R., and Liu, C.: Status of the TRMM 2A12 Land Precipitation Algorithm, *J. Atmos. Ocean. Tech.*, 27, 1343–1354, doi:10.1175/2010JTECHA1454.1, 2010.
- Goward, S. N. and Huemmrich, K. F.: Vegetation canopy PAR absorptance and the normalized difference vegetation index: An assessment using the SAIL model, *Remote Sens. Environ.*, 39, 119–140, doi:10.1016/0034-4257(92)90131-3, 1992.
- Grantz, K., Rajagopalan, B., Clark, M., and Zagona, E.: A technique for incorporating large-scale climate information in basinscale ensemble streamflow forecasts, *Water Resour. Res.*, 41, doi:10.1029/2004WR003467, 2005.
- Groot Zwaafink, C. D., Mott, R., and Lehning, M.: Seasonal simulation of drifting snow sublimation in Alpine terrain, *Water Resour. Res.*, 49, 1581–1590, doi:10.1002/wrcr.20137, 2013.
- Hall, D. K., Riggs, G. A., Salomonson, V. V., DiGirolamo, N. E., and Bayr, K. J.: MODIS snow-cover products, *Remote Sens. Environ.*, 83, 181–194, doi:10.1016/S0034-4257(02)00095-0, 2002.
- Hargreaves, G. H. and Samani, Z. A.: Reference Crop Evapotranspiration from Temperature, *Appl. Eng. Agric.*, 1, 96–99, doi:10.13031/2013.26773, 1985.
- HEC: Hydrologic Engineering Center (HEC) computer software for hydrologic engineering and planning analysis, available at: <http://www.hec.usace.army.mil/software/> (last access: 03 September 2014), 2014.
- Hewlett, J.: Soil moisture as a source of base flow from steep mountain watershed, Tech. rep., US forest Service, Southeastern Forest Experiment Station, Asheville, North Carolina, 1961.
- Heynen, M., Pellicciotti, F., and Carenzo, M.: Parameter sensitivity of a distributed enhanced temperature-index melt model, *Ann. Glaciol.*, 54, 311–321, doi:10.3189/2013AoG63A537, 2013.
- Hijmans, R. J., Cameron, S. E., Parra, J. L., Jones, P. G., and Jarvis, A.: Very high resolution interpolated climate surfaces for global land areas, *Int. J. Climatol.*, 25, 1965–1978, doi:10.1002/joc.1276, 2005.



- Hock, R.: Temperature index melt modelling in mountain areas, *J. Hydrol.*, 282, 104–115, doi:10.1016/S0022-1694(03)00257-9, 2003.
- Hock, R.: Glacier melt: a review of processes and their modelling, *Prog. Phys. Geog.*, 29, 362–391, doi:10.1191/0309133305pp453ra, 2005.
- Hooghoudt, S.: Bijdragen tot de kennis van eenige natuurkundige grootheden van den grond. No. 7. Algemeene beschouwing van het probleem van de detailontwatering en de infiltratie door middel van parallel loopende drains, greppels, slooten en kanalen, *Versl. Landbouwkd. Onderz.*, 46, 515–707, 1940.
- Hunink, J., Niadas, I., Antonaropoulos, P., Droogers, P., and de Vente, J.: Targeting of intervention areas to reduce reservoir sedimentation in the Tana catchment (Kenya) using SWAT, *Hydrolog. Sci. J.*, 58, 600–614, doi:10.1080/02626667.2013.774090, 2013.
- Immerzeel, W. and Droogers, P.: Calibration of a distributed hydrological model based on satellite evapotranspiration, *J. Hydrol.*, 349, 411–424, doi:10.1016/j.jhydrol.2007.11.017, 2008.
- Immerzeel, W., Lutz, A., and Droogers, P.: Climate Change Impacts on the Upstream Water Resources of the Amu and Syr Darya River Basins, Tech. rep., FutureWater, Wageningen, 2012.
- Immerzeel, W. and Bierkens, M. F. P.: Asia's water balance, *Nat. Geosci.*, 5, 841–842, doi:10.1038/ngeo1643, 2012.
- Immerzeel, W., Droogers, P., de Jong, S. M., and Bierkens, M. F. P.: Large-scale monitoring of snow cover and runoff simulation in Himalayan river basins using remote sensing, *Remote Sens. Environ.*, 113, 40–49, doi:10.1016/j.rse.2008.08.010, 2009.
- Immerzeel, W., van Beek, L. P. H., and Bierkens, M. F. P.: Climate change will affect the Asian water towers, *Science*, 328, 1382–1385, doi:10.1126/science.1183188, 2010.
- Immerzeel, W., Beek, L. P. H., Konz, M., Shrestha, A. B., and Bierkens, M. F. P.: Hydrological response to climate change in a glacierized catchment in the Himalayas, *Climatic Change*, 110, 721–736, doi:10.1007/s10584-011-0143-4, 2011.
- Irrisoft: Database and on-line Applications in Irrigation, Drainage & Hydrology, available at: <http://www.irrisoft.org> (last access: 07 May 2014), 2014.
- Karssenbergh, D.: The value of environmental modelling languages for building distributed hydrological models, *Hydrol. Process.*, 16, 2751–2766, doi:10.1002/hyp.1068, 2002.
- Karssenbergh, D., Burrough, P. A., Sluiter, R., and de Jong, K.: The PCRaster Software and Course Materials for Teaching Numerical Modelling in the Environmental Sciences, *T. GIS*, 5, 99–110, doi:10.1111/1467-9671.00070, 2001.
- Karssenbergh, D., Schmitz, O., Salamon, P., de Jong, K., and Bierkens, M. F.: A software framework for construction of process-based stochastic spatio-temporal models and data assimilation, *Environ. Model. Softw.*, 25, 489–502, doi:10.1016/j.envsoft.2009.10.004, 2010.
- Kauffman, S., Droogers, P., Hunink, J., Mwaniki, B., Muchena, F., Gicheru, P., Bindraban, P., Onduru, D., Cleveringa, R., and Bouma, J.: Green Water Credits – exploring its potential to enhance ecosystem services by reducing soil erosion in the Upper Tana basin, Kenya, *International Journal of Biodiversity Science, Ecosystem Services & Management*, 10, 133–143, doi:10.1080/21513732.2014.890670, 2014.
- Kokkonen, T., Koivusalo, H., Jakeman, A., and Norton, J.: Construction of a Degree-Day Snow Model in the Light of the “Ten Iterative Steps in Model Development”, in: *Proceedings of the iEMSs Third Biennial Meeting: Summit on Environmental Modelling and Software*, Environmental Modelling and Software Society, Burlington, USA, 2006.

- Kozak, J. A., Ahuja, L. R., Green, T. R., and Ma, L.: Modelling crop canopy and residue rainfall interception effects on soil hydrological components for semi-arid agriculture, *Hydrol. Process.*, 21, 229–241, doi:10.1002/hyp.6235, 2007.
- Krysanova, V., Müller-Wohlfeil, D.-I., and Becker, A.: Development and test of a spatially distributed hydrological/water quality model for mesoscale watersheds, *Ecol. Model.*, 106, 261–289, 1998.
- Krysanova, V., Wechsung, F., Arnold, J., Srinivasan, R., and Williams, J.: PIK Report Nr. 69 “SWIM (Soil and Water Integrated Model), User Manual”, Tech. rep., Potsdam Institute for Climate Impact Research, Potsdam, 2000.
- Krysanova, V., Hattermann, F., Huang, S., Hesse, C., Vetter, T., Liersch, S., Koch, H., and Kundzewicz, Z. W.: Modelling climate and land-use change impacts with SWIM: lessons learnt from multiple applications, *Hydrolog. Sci. J.*, 60, 606–635, doi:10.1080/02626667.2014.925560, 2015.
- Lall, U.: Debates – The future of hydrological sciences: A (common) path forward? One water. One world. Many climes. Many souls, *Water Resour. Res.*, 50, 5335–5341, doi:10.1002/2014WR015402, 2014.
- Lambert, J., Daroussin, J., Eimberck, M., Le Bas, C., Jamagne, M., King, D., and Montanarella, L.: Soil Geographical Database for Eurasia&The Mediterranean. Instructions Guide for Elaboration at scale 1:1,000,000 version 4.0. EUR 20422 EN., Tech. rep., JRC, Ispra, Italy, 2003.
- Lenaerts, J. T. M., van den Broeke, M. R., Déry, S. J., König-Langlo, G., Ettema, J., and Munneke, P. K.: Modelling snowdrift sublimation on an Antarctic ice shelf, *The Cryosphere*, 4, 179–190, doi:10.5194/tc-4-179-2010, 2010.
- Liang, X., Lettenmaier, D. P., Wood, E. F., and Burges, S. J.: A simple hydrologically based model of land surface water and energy fluxes for general circulation models, 99, 14415–14428, doi:10.1029/94JD00483, 1994.
- Liang, X., Wood, E. F., and Lettenmaier, D. P.: Surface soil moisture parameterization of the VIC-2L model: Evaluation and modification, *Global Planet. Change*, 13, 195–206, doi:10.1016/0921-8181(95)00046-1, 1996.
- Lindström, G., Pers, C., Rosberg, J., Strömqvist, J., and Arheimer, B.: Development and testing of the HYPE (Hydrological Predictions for the Environment) water quality model for different spatial scales, *Hydrol. Res.*, 41, 295–319, doi:10.2166/nh.2010.007, 2010.
- Liu, Y., Gupta, H., Springer, E., and Wagener, T.: Linking science with environmental decision making: Experiences from an integrated modeling approach to supporting sustainable water resources management, *Environ. Model. Softw.*, 23, 846–858, doi:10.1016/j.envsoft.2007.10.007, 2008.
- Lutz, A. F., Droogers, P., and Immerzeel, W.: Climate Change Impact and Adaptation on the Water Resources in the Amu Darya and Syr Darya River Basins, Tech. rep., FutureWater, Wageningen, 2012.
- Lutz, A. F., Immerzeel, W. W., Gobiet, A., Pellicciotti, F., and Bierkens, M. F. P.: Comparison of climate change signals in CMIP3 and CMIP5 multi-model ensembles and implications for Central Asian glaciers, *Hydrol. Earth Syst. Sci.*, 17, 3661–3677, doi:10.5194/hess-17-3661-2013, 2013.
- Lutz, A. F., Immerzeel, W. W., Shrestha, A. B., and Bierkens, M. F. P.: Consistent increase in High Asia’s runoff due to increasing glacier melt and precipitation, *Nature Climate Change*, 4, 587– 592, doi:10.1038/nclimate2237, 2014a.
- Lutz, A. F., Immerzeel, W., and Kraaijenbrink, P.: Gridded Meteorological Datasets and Hydrological Modelling in the Upper Indus Basin. FutureWater Report 130, Tech. rep., FutureWater, Wageningen, the Netherlands, 2014b.



- MacDonald, M. K., Pomeroy, J. W., and Pietroniro, A.: Parameterizing redistribution and sublimation of blowing snow for hydrological models: tests in a mountainous subarctic catchment, *Hydrol. Process.*, 23, 2570–2583, doi:10.1002/hyp.7356, 2009.
- Manning, R.: On the flow of water in open channels and pipes, *Trans. Inst. Civ. Eng. Ireland*, 20, 161–207, 1989.
- McPhee, J., Rubio-Alvarez, E., Meza, R., Ayala, A., Vargas, X., and Vicuna, S.: An approach to estimating hydropower impacts of climate change from a regional perspective, *Watershed Management*, 2010, 13–24, doi:10.1061/41143(394)2, 2010.
- Meehl, G. A., Covey, C., Taylor, K. E., Delworth, T., Stouffer, R. J., Latif, M., McAvaney, B., and Mitchell, J. F. B.: THE WCRP CMIP3 Multimodel Dataset: A New Era in Climate Change Research, *B. Am. Meteorol. Soc.*, 88, 1383–1394, doi:10.1175/BAMS-88-9-1383, 2007.
- Mendoza, P. A., McPhee, J., and Vargas, X.: Uncertainty in flood forecasting: A distributed modeling approach in a sparse data catchment, *Water Resour. Res.*, 48, W09532, doi:10.1029/2011WR011089, 2012.
- Morris, E. M. and Woolhiser, D. A.: Unsteady one-dimensional flow over a plane: Partial equilibrium and recession hydrographs, *Water Resour. Res.*, 16, 355–360, doi:10.1029/WR016i002p00355, 1980.
- Myneni, R. and Williams, D.: On the relationship between FAPAR and NDVI, *Remote Sens. Environ.*, 49, 200–211, doi:10.1016/0034-4257(94)90016-7, 1994.
- Nash, J. and Sutcliffe, J.: River flow forecasting through conceptual models part I – A discussion of principles, *J. Hydrol.*, 10, 282–290, doi:10.1016/0022-1694(70)90255-6, 1970.
- Neitsch, S. L., Arnold, J. G., Kiniry, J. R., and Williams, J. R.: Soil and Water Assessment Tool (SWAT). Theoretical Documentation, version 2009, Tech. rep., Texas Water Resources Institute, College Station, Texas, available at: <http://twri.tamu.edu/reports/2011/tr406.pdf> (last access: 04 June 2014), 2009.
- Niu, G. Y., Yang, Z. L., Mitchell, K. E., Chen, F., Ek, M. B., Barlage, M., Kumar, A., Manning, K., Niyogi, D., Rosero, E., Tewari, M., and Xia, Y.: The community Noah land surface model with multiparameterization options (Noah-MP): 1. Model description and evaluation with local-scale measurements, *J. Geophys. Res.- Atmos.*, 116, D12109, doi:10.1029/2010JD015139, 2011.
- Oogathoo, S., Prasher, S., Rudra, R., and Patel, R.: Calibration and validation of the MIKE SHE model in Canagagigue Creek watershed, in: *Agricultural and biosystems engineering for a sustainable world. International Conference on Agricultural Engineering*, Hersonissos, Crete, Greece, 2008.
- Parajka, J. and Blöschl, G.: Spatio-temporal combination of MODIS images – potential for snow cover mapping, *Water Resour. Res.*, 44, W03406, doi:10.1029/2007WR006204, 2008.
- Park, C. C.: World-wide variations in hydraulic geometry exponents of stream channels: An analysis and some observations, *J. Hydrol.*, 33, 133–146, doi:10.1016/0022-1694(77)90103-2, 1977.
- Pechlivanidis, I., Jackson, B., McIntyre, N., and Weather, H.: Catchment scale hydrological modelling: a review of model types, calibration approaches and uncertainty analysis methods in the context of recent developments in technology and applications, *Global NEST Journal*, 13, 193–214, 2011.
- Pellicciotti, F., Brock, B., Strasser, U., Burlando, P., Funk, M., and Corripio, J.: An enhanced temperature-index glacier melt model including the shortwave radiation balance: development and testing for Haut Glacier d’Arolla, Switzerland, *J. Glaciol.*, 51, 573–587, doi:10.3189/172756505781829124, 2005.



- Peng, D., Zhang, B., and Liu, L.: Comparing spatiotemporal patterns in Eurasian FPAR derived from two NDVI-based methods, *International Journal of Digital Earth*, 5, 283–298, doi:10.1080/17538947.2011.598193, 2012.
- Piechota, T. and Chiew, F.: Seasonal streamflow forecasting in eastern Australia and the El Niño – Southern Oscillation, *Water Resour. Res.*, 34, 3035–3044, 1998.
- Pomeroy, J. W., Gray, D. M., Brown, T., Hedstrom, N. R., Quinton, W. L., Granger, R. J., and Carey, S. K.: The cold regions hydrological model: A platform for basing process representation and model structure on physical evidence, *Hydrol. Process.*, 21, 2650–2667, doi:10.1002/hyp.6787, 2007.
- Rafn, E. B., Contor, B., and Ames, D. P.: Evaluation of a Method for Estimating Irrigated Crop-Evapotranspiration Coefficients from Remotely Sensed Data in Idaho, *J. Irrig. Drain. E.-ASCE*, 134, 722–729, doi:10.1061/(ASCE)0733-9437(2008)134:6(722), 2008.
- Ragetti, S. and Pellicciotti, F.: Calibration of a physically based, spatially distributed hydrological model in a glacierized basin: On the use of knowledge from glaciometeorological processes to constrain model parameters, *Water Resour. Res.*, 48, W03509, doi:10.1029/2011WR010559, 2012.
- Ragetti, S., Cortés, G., Mcphee, J., and Pellicciotti, F.: An evaluation of approaches for modelling hydrological processes in high elevation, glacierized Andean watersheds, *Hydrol. Process.*, 28, 5674–5695, doi:10.1002/hyp.10055, 2014.
- Ragetti, S., Pellicciotti, F., Immerzeel, W., Miles, E., Petersen, L., Heynen, M., Shea, J. M., Stumm, D., Joshi, S., and Shrestha, A.: Unraveling the hydrology of a Himalayan watershed through integration of high resolution in-situ data and remote sensing with an advanced simulation model, *Adv. Water Resour.*, 78, 94–111, doi:10.1016/j.advwatres.2015.01.013, 2015.
- Refshaard, J. and Storm, B.: MIKE SHE, Danish Hydraulic Institute, Horsholm, 1995.
- Regonda, S. K., Rajagopalan, B., Clark, M., and Zagona, E.: A multimodel ensemble forecast framework: Application to spring seasonal flows in the Gunnison River Basin, *Water Resour. Res.*, 42, W09404, doi:10.1029/2005WR004653, 2006.
- Reid, T. D., Carenzo, M., Pellicciotti, F., and Brock, B. W.: Including debris cover effects in a distributed model of glacier ablation, *J. Geophys. Res.-Atmos.*, 117, D18105, doi:10.1029/2012JD017795, 2012.
- Rigon, R., Bertoldi, G., and Over, T. M.: GEOTop: A Distributed Hydrological Model with Coupled Water and Energy Budgets, *J. Hydrometeorol.*, 7, 371–388, doi:10.1175/JHM497.1, 2006.
- Rockström, J., Falkenmark, M., Lannerstad, M., and Karlberg, L.: The planetary water drama: Dual task of feeding humanity and curbing climate change, *Geophys. Res. Lett.*, 39, L15401, doi:10.1029/2012GL051688, 2012.
- Rollenbeck, R. and Bendix, J.: Rainfall distribution in the Andes of southern Ecuador derived from blending weather radar data and meteorological field observations, *Atmos. Res.*, 99, 277–289, doi:10.1016/j.atmosres.2010.10.018, 2011.
- Samain, B., Simons, G. W. H., Voogt, M. P., Defloor, W., Bink, N.-J., and Pauwels, V. R. N.: Consistency between hydrological model, large aperture scintillometer and remote sensing based evapotranspiration estimates for a heterogeneous catchment, *Hydrol. Earth Syst. Sci.*, 16, 2095–2107, doi:10.5194/hess-16-2095-2012, 2012.
- Samaniego, L., Kumar, R., and Attinger, S.: Multiscale parameter regionalization of a grid-based hydrologic model at the mesoscale, *Water Resour. Res.*, 46, W05523, doi:10.1029/2008WR007327, 2010.
- Sangrey, D. A., Harrop-Williams, K. O., and Klaiber, J. A.: Predicting Ground-Water Response to Precipitation, *J. Geotech. Eng.-ASCE*, 110, 957–975, doi:10.1061/(ASCE)0733-9410(1984)110:7(957), 1984.



- Schaner, N., Voisin, N., Nijssen, B., and Lettenmaier, D. P.: The contribution of glacier melt to streamflow, *Environ. Res. Lett.*, 7, 034029, doi:10.1088/1748-9326/7/3/034029, 2012.
- Schmitz, O., Karssenber, D., van Deursen, W., and Wesseling, C.: Linking external components to a spatiotemporal modelling framework: Coupling MODFLOW and PCRaster, *Environ. Model. Softw.*, 24, 1088–1099, doi:10.1016/j.envsoft.2009.02.018, 2009.
- Schmitz, O., Karssenber, D., de Jong, K., de Kok, J.-L., and de Jong, S. M.: Map algebra and model algebra for integrated model building, *Environ. Model. Softw.*, 48, 113–128, doi:10.1016/j.envsoft.2013.06.009, 2013.
- Sellers, P. J., Tucker, C. J., Collatz, G. J., Los, S. O., Justice, C. O., Dazlich, D. A., and Randall, D. A.: A Revised Land Surface Parameterization (SiB2) for Atmospheric GCMS. Part II: The Generation of Global Fields of Terrestrial Biophysical Parameters from Satellite Data, *J. Climate*, 9, 706–737, doi:10.1175/1520-0442(1996)009<0706:ARLSPF>2.0.CO;2, 1996.
- Sheffield, J., Goteti, G., and Wood, E. F.: Development of a 50- Year High-Resolution Global Dataset of Meteorological Forcings for Land Surface Modeling, *J. Climate*, 19, 3088–3111, doi:10.1175/JCLI3790.1, 2006.
- Singh, P. and Kumar, N.: Impact assessment of climate change on the hydrological response of a snow and glacier melt runoff dominated Himalayan river, *J. Hydrol.*, 193, 316–350, doi:10.1016/S0022-1694(96)03142-3, 1997.
- Sloan, P. G. and Moore, I. D.: Modeling subsurface stormflow on steeply sloping forested watersheds, *Water Resour. Res.*, 20, 1815–1822, doi:10.1029/WR020i012p01815, 1984.
- Smedema, L. and Rycroft, D.: *Land Drainage: Planning and Design of Agricultural Drainage Systems*, Cornell University Press, 1983.
- Sorg, A., Bolch, T., Stoffel, M., Solomina, O., and Beniston, M.: Climate change impacts on glaciers and runoff in Tien Shan (Central Asia), *Nature Climate Change*, 2, 725–731, doi:10.1038/nclimate1592, 2012.
- Sperna Weiland, F. C., van Beek, L. P. H., Kwadijk, J. C. J., and Bierkens, M. F. P.: The ability of a GCM-forced hydrological model to reproduce global discharge variability, *Hydrol. Earth Syst. Sci.*, 14, 1595–1621, doi:10.5194/hess-14-1595-2010, 2010.
- Strasser, U., Bernhardt, M., Weber, M., Liston, G. E., and Mauser, W.: Is snow sublimation important in the alpine water balance?, *The Cryosphere*, 2, 53–66, doi:10.5194/tc-2-53-2008, 2008.
- Taylor, K. E., Stouffer, R. J., and Meehl, G. A.: An Overview of CMIP5 and the Experiment Design, *B. Am. Meteorol. Soc.*, 93, 485–498, doi:10.1175/BAMS-D-11-00094.1, 2012.
- Terink, W., A.F. Lutz, G.W.H. Simons, W.W. Immerzeel, P. Droogers. 2015. SPHY v2.0: Spatial Processes in HYdrology. *Geoscientific Model Development*, 8, 2009-2034, doi:10.5194/gmd-8-2009-2015.
- Terink, W., A.F. Lutz, G.W.H. Simons. 2015a. SPHY: Spatial Processes in HYdrology. Case-studies for training. *FutureWater report 144*.
- Terink, W., A.F. Lutz, W.W. Immerzeel. 2015b. SPHY: Spatial Processes in HYdrology. Graphical User-Interfaces (GUIs). *FutureWater report 143*.
- Tucker, C. J.: Red and photographic infrared linear combinations for monitoring vegetation, *Remote Sens. Environ.*, 8, 127–150, doi:10.1016/0034-4257(79)90013-0, 1979.
- USGS: Landsat 8: U.S. Geological Survey Fact Sheet 2013–3060, Tech. rep., available at: <http://pubs.usgs.gov/fs/2013/3060/> (last access: 15 June 2014), 2013.
- USGS: Water Resources Applications Software, available at: <http://water.usgs.gov/software/lists/alphabetical> (last access: 30 April 2014), 2014.



- van Beek, L. and Bierkens, M.: The Global Hydrological Model PCR-GLOBWB: Conceptualization, Parameterization and Verification, Tech. rep., Department of Physical Geography, Utrecht University, Utrecht, available at: <http://vanbeek.geo.uu.nl/suppinfo/vanbeekbierkens2009.pdf> (last access: 24 November 2014), 2008.
- van Dam, J. C., Huygen, J., Wesseling, J. G., Feddes, R. A., Kabat, P., van Walsum, P. E. V., Groenendijk, P., and van Diepen, C. A.: Theory of SWAP version 2.0. Simulation of water flow, solute transport and plant growth in the Soil-Water-Atmosphere-Plant environment, Tech. rep., Department Water Resources, Wageningen Agricultural University, 1997.
- Van Der Knijff, J. M., Younis, J., and De Roo, A. P. J.: LISFLOOD: a GIS-based distributed model for river basin scale water balance and flood simulation, *Int. J. Geogr. Inf. Sci.*, 24, 189–212, doi:10.1080/13658810802549154, 2010.
- Van Genuchten, M.: A closed-form equation for predicting the hydraulic conductivity of unsaturated soils, *Soil Sci. Soc. Am. J.*, 44, 892–898, 1980.
- VanderKwaak, J. E. and Loague, K.: Hydrologic-response simulations for the R-5 catchment with a comprehensive physics-based model, *Water Resour. Res.*, 37, 999–1013, doi:10.1029/2000WR900272, 2001.
- Venetis, C.: A STUDY ON THE RECESSION OF UNCONFINED ACQUIFERS, *International Association of Scientific Hydrology. Bulletin*, 14, 119–125, doi:10.1080/02626666909493759, 1969.
- Verbunt, M., Gurtz, J., Jasper, K., Lang, H., Warmerdam, P., and Zappa, M.: The hydrological role of snow and glaciers in alpine river basins and their distributed modeling, *J. Hydrol.*, 282, 36–55, doi:10.1016/S0022-1694(03)00251-8, 2003.
- Vicuña, S., Garreaud, R. D., and McPhee, J.: Climate change impacts on the hydrology of a snowmelt driven basin in semiarid Chile, *Climatic Change*, 105, 469–488, doi:10.1007/s10584-010-9888-4, 2011.
- Von Hoyningen-Huene, J.: Die Interzeption des Niederschlags in landwirtschaftlichen Pflanzenbeständen, *Arbeitsbericht Deutscher Verband für Wasserwirtschaft und Kulturbau, DWK*, 1981.
- Wada, Y., Van Beek, L. P. H., Van Kempen, C. M., Reckman, J. W. T. M., Vasak, S., and Bierkens, M. F. P.: Global depletion of groundwater resources, *Geophys. Res. Lett.*, 37, L20402, doi:10.1029/2010GL044571, 2010.
- Wagener, T., Sivapalan, M., Troch, P. A., McGlynn, B. L., Harman, C. J., Gupta, H. V., Kumar, P., Rao, P. S. C., Basu, N. B., and Wilson, J. S.: The future of hydrology: An evolving science for a changing world, *Water Resour. Res.*, 46, W05301, doi:10.1029/2009WR008906, 2010.
- Wagner, P. D., Fiener, P., Wilken, F., Kumar, S., and Schneider, K.: Comparison and evaluation of spatial interpolation schemes for daily rainfall in data scarce regions, *J. Hydrol.*, 464–465, 388–400, doi:10.1016/j.jhydrol.2012.07.026, 2012.
- Wheeler, T. and von Braun, J.: Climate change impacts on global food security, *Science*, 341, 508–513, doi:10.1126/science.1239402, 2013.
- Wigmosta, M. S., Vail, L. W., and Lettenmaier, D. P.: A distributed hydrology-vegetation model for complex terrain, *Water Resour. Res.*, 30, 1665–1680, doi:10.1029/94WR00436, 1994.
- Williams, J.: HYMO flood routing, *J. Hydrol.*, 26, 17–27, doi:10.1016/0022-1694(75)90122-5, 1975.
- Yatagai, A., Kamiguchi, K., Arakawa, O., Hamada, A., Yasutomi, N., and Kitoh, A.: APHRODITE: Constructing a Long-Term Daily Gridded Precipitation Dataset for Asia



Based on a Dense Network of Rain Gauges, B. Am. Meteorol. Soc., 93, 1401–1415,
doi:10.1175/BAMS-D-11-00122.1, 2012.



Copyright

Redistribution and use of the SPHY model source code or its binary forms, with or without modification, are permitted provided that the following conditions are met:

1. Redistributions of source code must retain this copyright notice, this list of conditions and the following disclaimer.
2. Redistributions in binary form must reproduce the above copyright notice, this list of conditions and the following disclaimer in the documentation and/or other materials provided with the distribution.
3. Any changes, modifications, improvements and/or simplifications of the source code should be sent to FutureWater.
4. Any redistribution of source code or binary form should be reported to FutureWater.
5. Any application, publication and/or presentation of results generated by using the Software should be reported to FutureWater.

THIS SOFTWARE IS PROVIDED BY THE COPYRIGHT HOLDERS AND CONTRIBUTORS "AS IS" AND ANY EXPRESS OR IMPLIED WARRANTIES, INCLUDING, BUT NOT LIMITED TO, THE IMPLIED WARRANTIES OF MERCHANTABILITY AND FITNESS FOR A PARTICULAR PURPOSE ARE DISCLAIMED. IN NO EVENT SHALL THE COPYRIGHT OWNER OR CONTRIBUTORS BE LIABLE FOR ANY DIRECT, INDIRECT, INCIDENTAL, SPECIAL, EXEMPLARY, OR CONSEQUENTIAL DAMAGES (INCLUDING, BUT NOT LIMITED TO, PROCUREMENT OF SUBSTITUTE GOODS OR SERVICES; LOSS OF USE, DATA, OR PROFITS; OR BUSINESS INTERRUPTION) HOWEVER CAUSED AND ON ANY THEORY OF LIABILITY, WHETHER IN CONTRACT, STRICT LIABILITY, OR TORT (INCLUDING NEGLIGENCE OR OTHERWISE) ARISING IN ANY WAY OUT OF THE USE OF THIS SOFTWARE, EVEN IF ADVISED OF THE POSSIBILITY OF SUCH DAMAGE.



Appendix 1: Input and Output

Table 6: Overview of SPHY model parameters. The last column indicates whether the parameter is observable, or can be determined by calibration (free).

Acronym	Description	Units	Parameter determination
Kc	Crop coefficient	–	Free
Kc _{max}	Maximum crop coefficient	–	Free
Kc _{min}	Minimum crop coefficient	–	Free
NDVI _{max}	Maximum NDVI	–	Observable
NDVI _{min}	Minimum NDVI	–	Observable
FPAR _{max}	Maximum fraction of absorbed photosynthetically active radiation	–	Free
FPAR _{min}	Minimum fraction of absorbed photosynthetically active radiation	–	Free
T _{crit}	Temperature threshold for precipitation to fall as snow	°C	Free
DDF _s	Degree-day factor for snow	mm °C ⁻¹ day ⁻¹	Free
SSC	Water storage capacity of snowpack	mm mm ⁻¹	Free
GlacF	Glacier fraction of grid cell	–	Observable
DDF _{CI}	Degree-day factor for debris-free glaciers	mm °C ⁻¹ day ⁻¹	Free
DDF _{DC}	Degree-day factor for debris-covered glaciers	mm °C ⁻¹ day ⁻¹	Free
F _{CI}	Fraction of GlacF that is debris free	–	Observable
F _{DC}	Fraction of GlacF that is covered with debris	–	Observable
GlacROF	Fraction of glacier melt that becomes glacier runoff	–	Free
SW _{1,sat}	Saturated soil water content of first soil layer	mm	Observable
SW _{1,fc}	Field capacity of first soil layer	mm	Observable
SW _{1,pF3}	Wilting point of first soil layer	mm	Observable
SW _{1,pF4.2}	Permanent wilting point of first soil layer	mm	Observable
K _{sat,1}	Saturated hydraulic conductivity of first soil layer	mm day ⁻¹	Observable
SW _{2,sat}	Saturated soil water content of second soil layer	mm	Observable
SW _{2,fc}	Field capacity of second soil layer	mm	Observable
K _{sat,2}	Saturated hydraulic conductivity of second soil layer	mm day ⁻¹	Observable
SW _{3,sat}	Saturated soil water content of groundwater layer	mm	Observable
slp	Slope of grid cell	m m ⁻¹	Observable
δ _{gw}	Groundwater recharge delay time	day	Free
α _{gw}	Baseflow recession coefficient	day ⁻¹	Free
BF _{fresh}	Threshold for baseflow to occur	mm	Free
kx	Flow recession coefficient	–	Free

